Stockholm University

Bachelor Thesis

Degree Project in Geochemistry 15 hp

Biomarker evidence for changing monsoon intensity in maar lakes Twin Ma and Taung Pyauk, central Myanmar

Francis Matthews

Stockholm 2018

Department of Geological Sciences
Stockholm University
SE-106 91 Stockholm
Sweden

Abstract

Myanmar's monsoonal climate is comparatively understudied considering the high societal, economical and agricultural dependence on the annual rainfall source it provides. Two maar lake sediment cores (Twin Ma and Taung Pyauk) in central Myanmar were analysed using *n*-alkane and bulk organic stable ^{13}C and ^{15}N isotopic proxies, with the aim of understanding high and low frequency teleconnection driven variability in monsoon intensity. A 100-year sedimentary *n*-alkane record was combined with a regional instrumental climatic dataset to infer climatically instigated shifts in OM sources and characteristics in Twin Ma over modern timescales. Inferences made were applied to a 1500-year (Taung Pyauk) *n*-alkane, TOC, $^{13}C_{TOC}$ and $^{15}N_{TOC}$ record to identify potentially long periodic oscillations in monsoon intensity. Changes in *n*-alkane distribution suggest periodic shifts away from the normal allochthonous terrestrially derived OM (high ACL, CPI) towards a highly productive algal/macrophyte dominated trophic state (lower ACL, CPI and increased C_{23}, C_{19}). In both lakes, this is likely prompted by drier periods (weaker monsoon intensity) with a low waterbody level, possibly related to negative PDO phases. These *n*-alkane distribution phases accompanied higher TOC and $^{13}C_{TOC}$ content in Taung Pyauk, indicating cyanobacterial blooms utilising isotopically heavier bicarbonate ions in a warmer, CO_2 limited pool. The occurrence of these phenomena over a spectrum of timescales, ranging from quasi-periodic (sub 20-years) in Twin Ma, to quasi-centennial (75 to 115-years) and pentadecadal (50 to 70-years) in Taung Pyauk suggests short and long-term teleconnection patterns dictate monsoon intensity with notable environmental change.

Bachelor thesis in Geochemistry 15 hp
Francis Matthews
Supervised by Rienk Smittenberg, Department of Geological Sciences, Stockholm University.

Table of Contents

1. Introduction

Present-day Myanmar (formerly Burma) is vulnerable to climate and environmental extremities capable of testing the resilience of its agriculturally dominated economy in response to intense drought and flooding (D'Arrigo and Ummenhofer, 2014). The dependency of southern Asia on the Indian summer monsoon is profound, contributing as much as 90 % to the annual precipitation budget (Htway and Matsumoto, 2011). Societal dependence on monsoonal rainfall make potential perturbations in its intensity a threat for both human life and agricultural production in a region that has received comparatively little climatological attention. Consequently, recent focus has aimed at deciphering the impact of spatial and temporally variability of major teleconnections such as the periodic Indian Ocean Dipole mode (IOD), Pacific Decadal Oscillation (POD) and El Niño-Southern Oscillation (ENSO) on the overlapping annual monsoonal system in Myanmar (D'Arrigo et al., 2011; D'Arrigo and Ummenhofer, 2014). Analysis of decadal data series by Sen Ron and Sen Roy, (2009) emphasised the complex interlinking between the ENSO and PDO; with precipitation suppressed during El Niño years, modulated by the PDO and causing drought conditions in combined El Niño/warm PDO years and wet conditions during La Niña/cold PDO.

Interpreting past effects of monsoonal variability on the hydrological landscape and biosphere represents a critical link in understanding the consequences of perturbations in natural climate phenomena. Additionally, understanding natural variability in the climatic regime of Myanmar helps to build a consensus as to the level of modern day change attributable to anthropogenic activities.

Maar crater lakes form through phreatomagmatic eruptions and provide a unique record of climatic oscillation due to their endorheic nature; balanced exclusively by rainfall and evaporation in a small crater catchment (Ortiz et al., 2013). Furthermore, high organic matter (OM) accumulation rates, in combination with a seasonally to permanently anoxic hypolimnion favors the intact preservation of a high temporal resolution stratigraphic record (Allen et al., 1999). Organic geochemical proxies provide a mechanism through which non-labile compounds can be analysed to infer a paleoenvironmental signal from a composite mixture of depositing matter (Meyers, 2003). Combining analysis of *n*-alkanes and stable isotopes in the organic geochemical record can discern useful information retained post-diagenesis; regarding dominant OM sources, biosynthesis pathways, waterbody and climatological characteristics (Freeman and Pancost, 2014).

The aim of this thesis is to provide what is probably the first preliminary analysis of monsoon induced OM source changes within 2 maar crater lakes (Twin Ma and Taung Pyauk) in central Myanmar. This was objectively undertaken by comparing a 100-year Twin Ma *n*-alkane record with a representative climatic (temperature, precipitation) dataset. Inferences were combined with stable isotopic analysis ($\delta^{13}C_{TOC}$, $\delta^{15}N_{TOC}$) to deduce monsoonal changes over a longer 1500-year period in the adjacent lake Taung Pyauk.

1.2. Aliphatic *n*-alkane proxies

Epicuticular *n*-alkane waxes (C_nH_{2n+2}) represent a group of ubiquitous, highly stable, straight chained and saturated hydrocarbon compounds operating as a modifiable extracellular cuticle boundary to environmental stresses (Dominguez et al., 2011). Contributing sources to lacustrine basins are bacteria, algae, aquatic macrophytes and terrestrial plants (Ortiz et al., 2013). The resistance of *n*-alkanes to diagenetic breakdown causes the sedimentary archive to closely match the depositional composition (Bianchi and Canuel, 2011). Homologue distribution of *n*-alkanes is an established proxy for measuring changes in OM source within complex depositional environments. Proxies have been developed and applied to discern both active OM source spatial distribution in sedimentary basins (Mead et al., 2005; Fang et al., 2014; Zhang et al., 2013) and as a paleoclimatic proxy to measure terrestrial and aquatic OM input variation through time (Brincat et al., 2000; Zech et al 2013).

Average chain length (ACL) is a proxy applied to distinguish between OM sources according to dominant chain lengths and corresponds to a weighted average of carbon chain lengths by concentration within a sample (Simoneit et al., 1991).

$$ACL = \frac{(23 \times C_{23} + 25 \times C_{25} + 27 \times C_{27} + 29 \times C_{29} + 31 \times C_{29} + 33 \times C_{33})}{C_{23} + C_{25} + C_{27} + C_{29} + C_{31} + C_{33}} \quad \text{(Eq.1)}$$

Where C_x is the individual *n*-alkane homologue concentration. Terrestrial vegetation possesses a long chain dominated *n*-alkane distribution (>27), whereas aquatic macrophytes contain a mid-chain length dominance (C_{21}, C_{23} and C_{25}) and phytoplankton exhibit a short chain (C_{17} and C_{19}) dominance (Ficken et al., 2000). Additionally, increasing ACL has been used to imply increased relative dominance of C_4 over C_3 photosynthetic pathways in response to C_4 grass species

expansion in arid climates over geological timescales (Vogts et al., 2012). On shorter timescales, ACL in vegetation is proposed to increase in response to a longer growing season regardless of the adopted photosynthetic pathway (Bush and McInerney 2015). Thus, ACL interpretation can be rewarding but complex due to postulated variation with climate, photosynthetic species composition, as well as natural and anthropogenic addition of petrogenic hydrocarbons (Ahad et al., 2011).

The Paq index was developed by Ficken et al., (2000) based on the characteristic suite of *n*-alkanes possessed by macrophyte groups. The index permits the differentiation of submerged macrophytes, emergent macrophytes and terrestrial vegetation through their increasing dominance of long chain *n*-alkanes respectively.

$$Paq = (C_{23} + C_{25}) / (C_{23} + C_{25} + C_{31} + C_{33}) \quad \text{(Eq.2)}$$

Paq values < 0.1 correspond to terrestrial vegetation, 0.1 - 0.4 to emergent macrophytes and 0.4 - 1 indicates submerged/floating macrophytes. As the sedimentary archive represents a mixture of OM sources, it is conceivable that middle range Paq values (0.1 - 0.4) represent average mixtures of all OM components so care is required in interpretation (Ficken et al., 2000). The Paq index strongly negatively correlates with ACL index when the Paq input chain lengths are those that dominate the homologues of the ACL, as is typically the case in natural *n*-alkane distributions.

The carbon preference index (CPI) gives a quantitative measure of the natural biological preference for odd over even numbered *n*-alkane carbon chain length, typical of a taxonomically higher plant contribution (Marzi et al., 1993).

$$CPI = 0.5\left(\frac{(C_{23} + C_{25} + C_{27} + C_{29} + C_{31})(C_{25} + C_{27} + C_{29} + C_{31} + C_{33}}{(C_{24} + C_{26} + C_{28} + C_{30} + C_{32})}\right) \quad \text{(Eq.3)}$$

A CPI of 1 represents a basal threshold for *n*-alkane odd over even chain length preference. High CPI values are a widespread occurrence in most modern-day plants, allowing its application as an indicator of terrestrial OM input (Bush and McInerney, 2013). Naturally high CPI values arise in higher plants due to the dominant biosynthetic pathway being the decarboxylation of even numbered alkyl-acids, forming predominantly odd chained n-alkanes (Bianchi and Canuel, 2011). Conversely, CPI values closer to and below 1 can indicate increased microorganism input, recycled OM or petrogenic hydrocarbon sources (Kennicutt et al., 1987).

1.3. Stable ^{13}C and ^{15}N isotope proxies in bulk organic matter

Bulk total organic matter (TOM) $\delta^{13}C$ and $\delta^{15}N$ can provide valuable information about the integrated biomass within lakes. Bulk TOM stable isotopic analysis allows a practical way to distinguish dominant OM sources and imply changes in lacustrine environments related to OM source transitions, lake productivity or changes in OM burial and recycling processes (Lui et al., 2013). The preference for lighter stable isotopes (i.e. ^{12}C, ^{14}N) during the enzymatic reactions of biosynthesis creates a measurable depletion in the ratio of heavy to light isotopes between the inorganic substrate and organic product (Bianchi and Canuel, 2011). For example, the magnitude of discrimination against ^{13}C is dependent on the fractionation factor (α):

$$\alpha = R_p \,/\, R_s$$

(Eq.4)

Where R_p is the assimilated product and R_S the obtained substrate. In stable carbon isotopic fractionation, the overall factor (Δ) is modelled in the C_3 biosynthesis pathway under constant ambient $\delta^{13}C$ CO_2 values as:

$$\delta c_3 = \delta co_2 - a - (b - a)c_i \,/\, c_a$$

(Eq.5)

Where δCO_2 is the $\delta^{13}C$ of ambient atmospheric CO_2, a is the isotopic fractionation effect from stomatal diffusion (- 4.4 ‰) (O'Leary, 1988), b is the isotopic effect of RuBP and phosphoenolpyruvate (PEP) carboxylases within the Calvin cycle (- 27 ‰), and $c_i \,/\, c_a$ is the concentration ratio of CO_2 inside to the plant compared to the outside atmosphere (Bianchi and Canuel, 2011; Freeman and Pancost, 2014). Thus, enzymatic related fractionation dominates overall, though less discriminatory diffusional fractionation predominates as CO_2 becomes limiting. Changes in bulk TOM $\delta^{13}C$ in a lacustrine body can be ascribed to the relative abundance of C_3 vs C_4 plants within a source area. C_4 plants are much less phylogenetically rich but have a considerably higher average $\delta^{13}C$ value owing to their utilisation of the Hatch-Slack assimilatory pathway in arid conditions (Chikaraishi, 2014). Other factors causing less negative $\delta^{13}C$ values

within the more abundant C_3 (Calvin-Benson assimilatory pathway) species are; temperature, utilization of HCO_3^- instead of CO^2 in aquatic environments, lower terrestrial moisture availability and light intensity (Freeman and Pancost, 2014 and references therein).

2. Study Site

Twin Ma and Taung Pyauk (22°17'N, 94°58'E) are two adjacent maar crater lakes of 31 m and 8 m depth respectively, formed through early quaternary alkali basaltic phreatomagmatic eruptions (Fig. 1). Both sampled lakes are situated west of the Sagaing transverse fault, dividing the Indian and Sunda continental plates (Sun et al., 2016). The crater lakes are situated on the western bank of the Chindwin River within the arid Central Myanmar zone of homogenous rainfall, defined by Sen Roy and Kaur (2000) as the area with the lowest average annual precipitation in Myanmar. Low rainfall is attributed to the orographic rain shadow effect of the eastern Shan plateau and western Rakhine Yoma Mountains blocking the passage of air masses from the Pacific and Indian Oceans respectively (Sun et al., 2016). The climate is tropical Savannah with a mean annual air temperature of 27 °C and a strongly seasonal rainfall input dominated (90%) by the monsoon rainfall between its onset in the middle of May and withdrawal at the beginning of October (Htway and Matsumoto, 2011).

Twin Ma and Taung Pyauk are highly alkaline (pH 10-11) soda lakes with strong stratification producing anoxic conditions below several meters water depth. Both are roughly circular lakes with waterbody surface areas of approximately 0.53 km^2 and 0.38 km^2 and catchment areas of 2.1 km^2 and 1.0 km^2 respectively, with vegetated waterbody perimeters. Both lakes have natural *Spirulina* algae blooms occurring in the dry season between February and April that are economically harvested as a medicinal product in Twin Ma. Algal blooming and high evaporation in the dry season have been observed by Sun et al., (2016) to induce authigenic calcium carbonate precipitation and varve formation in the adjacent Twintuang crater lake.

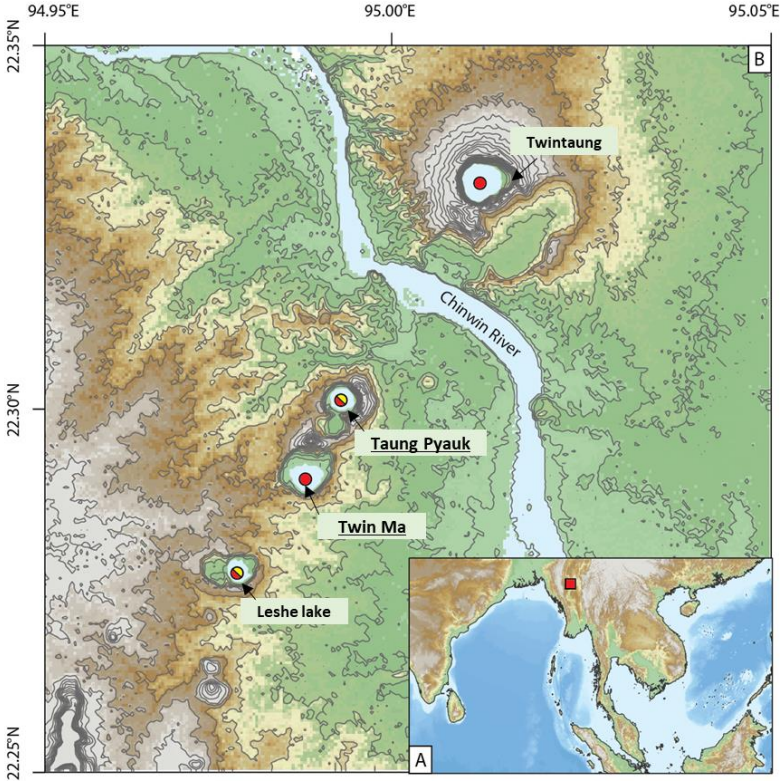

Figure 1. Study sites of both sampled crater lakes in central Myanmar. Map (A) represents the general location of studied Maar crater lakes in southern Asia. Map (B) depicts the 4 clustered crater lakes, 2 of which (Twin Ma and Taung Pyauk) featured in this study. Credit A. Chabangborn.

3. Methodology

All stages of subsampling, lipid extraction, fractionation and gas chromatography – mass spectrometry (GC-MS) analysis were undertaken on the 70 cm Twin Ma core whereas lipid extraction was already previously completed on the 170 cm Taung Pyauk core, therefore only GC-MS analysis was undertaken on the 79 pre-prepared samples (roughly every other sample). Taung Pyauk was previously analysed before this study for %TOC, δ^{13}C-org and δ^{15}N-org, taken at 2 cm intervals using a Carlo Erba NC2500 elemental analyser coupled to a Finnigan MAT Delta + mass spectrometer. Prior to sampling, sediment was freeze-dried and homogenized without prior removal of carbonate carbon as the observed quantity was low. Both δ^{13}C and δ^{15}N were measured in ‰ using a Vienna PeeDee Belemnite (VPDB) and AIR respectively.

3.1. Coring extraction, subsampling and radiocarbon dating

Two sediment cores were taken in November 2013 during a Stockholm University research expedition to Myanmar, northwest Indo-China Peninsula, from Twin Ma and Taung Pyauk maar crater lakes (Appendix. 1). A 70 cm depth core was extracted from Twin Ma (31 m depth) center using an HTK corer assembled with a 10 cm diameter PVC tube. From Taung Pyauk, a 170 cm depth core was extracted using a 1 m long Russian corer (7.5 cm diameter) overlapped to give a continuous long section of 170 cm. Both cores were returned to Stockholm University and remained sealed inside the core liner within a cool room (4°C) for later subsampling and lipid extraction.

The Twin Ma core was opened using a non-destructive core splitter and separated in half using a metal wire. One core half was wrapped in plastic film for preservation and the second half was laterally face cleaned for intact stratigraphic analysis. Liner-sediment separation resulted in a detachment of the bulk inner sediment (A) and sediment attached to the lining (B); each was individually subsampled at 1 cm intervals and stored in TEFLON containers at 4°C (Appendix. 2). Every other sample of subsample A was freeze dried for further lipid extraction and fractionation.

Taung Pyauk radiocarbon dating was undertaken prior to this thesis study by staff at Stockholm University. A number a sediment samples were sieved and macrofossils selected using a microscope by B.Wohlfarth. Samples were washed with milliQ water and submitted to the Radiocarbon facility at ETH Zurich, Switzerland for radiocarbon analysis. There, samples were pre-treated and analysed for radiocarbon content using a MIDACAS system equipped with a gas source. Radiocarbon ages were calibrated using the Oxcal v, 4.3 program provided by the University of Oxford (Bronk Ramsey, 2009a), the IntCal13 calibration curve (Reimer et al, 2013), and the U_sequence deposition model (Bronk Ramsey, 2008). The upper sample was identified as a clear outlier (Table. 1).

Table 1. Radiocarbon dating results from Taung Pyauk calibrated using the IntCal13 curve, with associated dates and uncertainty range.

	Sample type	Core depth	14c age (yr)	Uncertainty (±yr)
	Leaf fragment, charcoal,	871-870	1569	75
	Leaf fragment, charred plant material	896-895	307	73
	Leaf fragment, charred plant material	921-920	651	73
	Leaf fragment, charred plant material	946-945	1167	72
	Leaf fragment, charred plant material	971-970	1085	74
	Charred plant material	996-995	1482	80

Each sample of Twin Ma was rooted for macrofossils by hand during the sediment subsampling process. Three macrofossils were extracted, washed with milliQ water, oven dried and submitted to the Ångström laboratory at Uppsala University where they were pre-treated and analysed with a graphite source equipped MICADAS system. Radiocarbon contents were identified as modern and therefore calibrated with the Oxcal v, 4.3 program, but calibration was undertaken using the Bomb13NH3 calibration curve suited for the Northern hemisphere mean summer intertropical convergence zone (Hua et al., 2013). The upper sample was identified as an outlier and therefore a chronological record was extrapolated linearly from the two available radiocarbon dates (Table. 2).

Table 2. Radiocarbon dating results from Twin Ma calibrated using the Bomb13NH3 curve, with associated dates and uncertainty range.

	Sample type	Core depth (cm)	14C (pmC)	Uncertainty (±)
	thin leaf/rootlet	11-12	105.4	0.5
	thin leaf/rootlet	21-22	107.0	0.5
	thin leaf/rootlet	34-35	155.0	0.5

3.2. Spectrophotometry and SEM analysis

Spectrophotometry and SEM data was collected on the intact Twin Ma core before subsampling. The sediment core face was photographed and quantitatively analysed using a handheld spectrophotometer. The CIE (Commission Internationale de l' Éclairage) colour index's (L*, a*, b*) and total colour change (∆E) were plotted to quantify changes in each parameter at 2 cm intervals throughout the core depth as a proxy for mineral variation (Balsam et al., 1999; Nederbragt et al., 2006). Where ∆E is:

$$\Delta E = \sqrt{(L_2^* - L_1^*)^2 + (a_2^* - a_1^*)^2 + (b_2^* - b_1^*)^2} \quad \text{(Eq.6)}$$

L* is luminescence or lightness, a* is red-green index (positive values greener) and b* is blue-yellow index (positive values more yellow) at respective depths 2 and 1, giving change in total colour (E) at 2 cm intervals through the middle of the core.

Due to the homogeneity of the sediment core, 2 representative samples were taken for scanning electron microscopy analysis (SEM) to initially examine mineral type, structure and elemental composition and to test for the presence of authigenic carbonates. Sediment samples were placed on thin sections for analysis without a metallic resin coating for initial analysis, but image quality was sufficient for mineral identification. The backscatter electron (BSE) component results were not taken as accurately representative of the average atomic number of the target owing to the absence of a sample metallic coating. The secondary electron imagery (SEI) and X-ray microanalysis components were used to produce mineral topographic imagery and to map elemental composition respectively. The reader is directed to Pike and Kemp (1996) for a more substantive overview of the SEM procedure.

3.2. Lipid extraction and fractionation

Freeze dried samples were ground into a fine powder and weighed in pre-combusted 40 ml glass tubes. Lipid extraction was performed using a dichloromethane/methanol (9:1 v/v) solvent mix. Samples were sonicated for 15 minutes at room temperature and centrifuged for 10 minutes at 2500 rpm and 6 degrees. The lipid extraction phase was repeated 3 times and the supernatant

extracted each time until a total lipid extract (TLE) was obtained after solvent was evaporated using blown nitrogen gas.

The TLE was dissolved in approximately 3 ml of dichloromethane, dried and bound to silica gel for fractionation on silica gel columns. Four fractionations were eluted using; *n*-hexane (F1), *n*-hexane/dichloromethane (1:1 v/v, F2), dichloromethane/methanol (1:1 v/v, F3) and methanol (F4) and dry lipid extractions were frozen and stored. Fraction 1 (neutral aliphatic hydrocarbon phase) was further treated for Sulphur using columns activated copper, pre-rinsed using hydrochloric acid, isopropyl and *n*-hexane.

3.3. GCMS analysis

The neutral aliphatic hydrocarbon fraction (F1) of both lakes was analysed and quantified using GC-MS. Samples were dissolved in 500 µl of *n*-hexane for analysis using a Shimadzu GCMS-QP2010 ultra machine equipped with an AOC-20i auto sampler and a split-splitless injector operated in splitless mode. A Zebron ZB-5HT Inferno GC column (30 m length, 0.25 mm inner diameter, 0.25 µm film thickness) was used to separate the analyte volatile components. The GC oven was programmed to heat at 20°C min^{-1} starting at 60°C, to 180°C, after which the temperature was increased to 320°C at 4°C min^{-1}, followed by a 30-minute isothermal phase. The carrier gas used was helium with a 1 ml min^{-1} continuous flow rate. The MS operating system ion source was set to 200 °C and 70 eV ionization energy.

The *n*-alkane concentration per sample was calculated using a calibration with 3 external standards of 2, 4 and 8 ng containing C_{21}-C_{40} chain lengths places at the start, end and intermittently throughout the sample series. Peak area was undertaken with Shimadzu GCMSSolution v 2.6 software to integrate *n*-alkane total ion current through an automated method using standard retention times and literature referenced ion mass fragments (71 and 57). Erroneous peaks that were incorrectly quantified due to the presence of an unresolved complex mixture (UCM) or that were incompletely resolved were integrated manually. Other biomarkers of interest were identified (Appendix. 3), and peak area quantified using an analogous method adopting individual compound characteristic reference ions. In the absence of a standard for each biomarker, quantification was undertaken by normalizing TIC peak area by the sample weight (g). A more comprehensive description of the GCMS post-run analysis is available in (Appendix. 4).

3.4. Data analysis and comparison with climatological trend

Changes in *n*-alkane distribution were determined through changes in ACL, Paq and CPI indices using the dominant *n*-alkane homologues (C_{23}-C_{33}), calculated via Eq. (1, 2 & 3). Short chain *n*-alkanes (> C_{21}) were analysed separately due to their lower abundance and intermittent absence. Statistical correlation between parameters was undertaken using Pearson's correlation coefficient (r) after a normal distribution was established. Spearman's correlation (r_S) was used as a non-parametric alternative if the assumption of normality was failed after a Shapiro-Wilk normality test was undertaken with a critical p (normal) of 0.05 (Appendix. 5). Statistical analysis was undertaken using PAST Hammer et al., (2001).

Twin Ma *n*-alkane indices were compared against a representative 115-year long CRU TS 4.01 observational climate (temperature, precipitation) dataset compiled by Harris et al., (2014). Climatological data was available at a half degree cell resolution, thus the cell centered at 22°25'N, 95°25'E was taken as a representative dataset. Data was compiled into 3-year segments (January – December) for testing against *n*-alkane distribution at a comparable resolution.

4. Results

4.1. Twin Ma core description and spectrophotometry results

The Twin Ma sediment core was organically rich throughout and displayed a nearly homogenous grey coloured mineralogical composition dominated by clay and very fine silt grain size, with no evident mineral stratigraphy throughout the 70 cm core length (Fig. 2). Sediment was dark and iron sulfide (FeS) rich throughout which began oxidizing upon exposure to oxygen after core opening, forming intermittent orange iron banding. Some localized areas of FeS or organic material enrichment displayed darker patches that later oxidized.

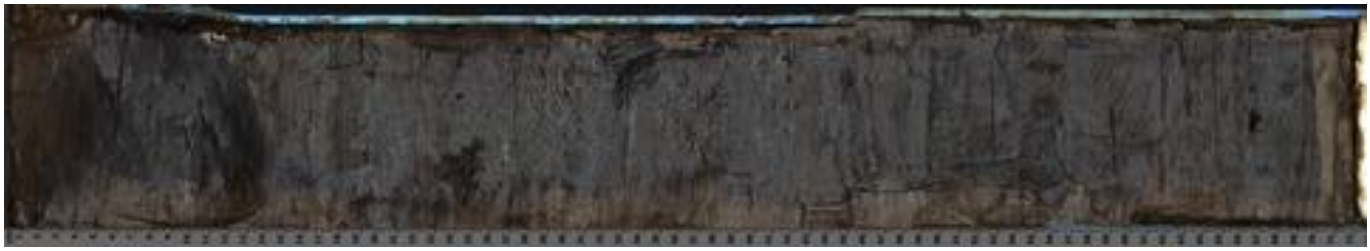

Figure 2. Twin Ma photographed core. Note, sediment core was not fully oxidized during the time of photography therefore most colour difference is attributed to oxidation state.

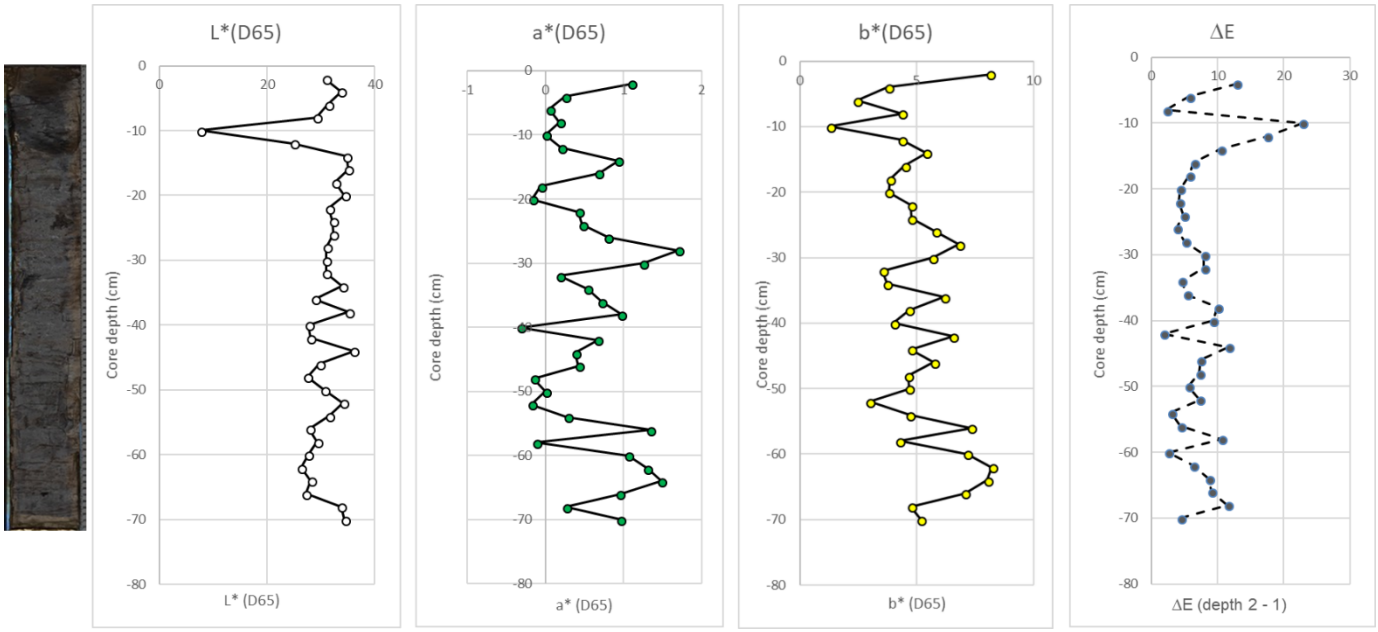

Figure 3. Spectrophotometry analysis showing changes in L* (lightness), a* (greenness), b* (yellowness) and total colour change (ΔE) throughout Twin Ma sediment core.

Spectrophotometry produced limited use for interpretation due to differences in oxidation status throughout the core. Data displayed some intermittent change in total colour (ΔE) with depth but little stratigraphic layering was evident (Fig. 3). Some variance in lightness (L*) through the core with lower values corresponding to the darkest patches of sediment, evidenced at 10 cm depth. Higher values of a* and b* occurred at intermittent depths layers of more green/yellow sediment.

4.2. Twin Ma scanning electron microscopy results

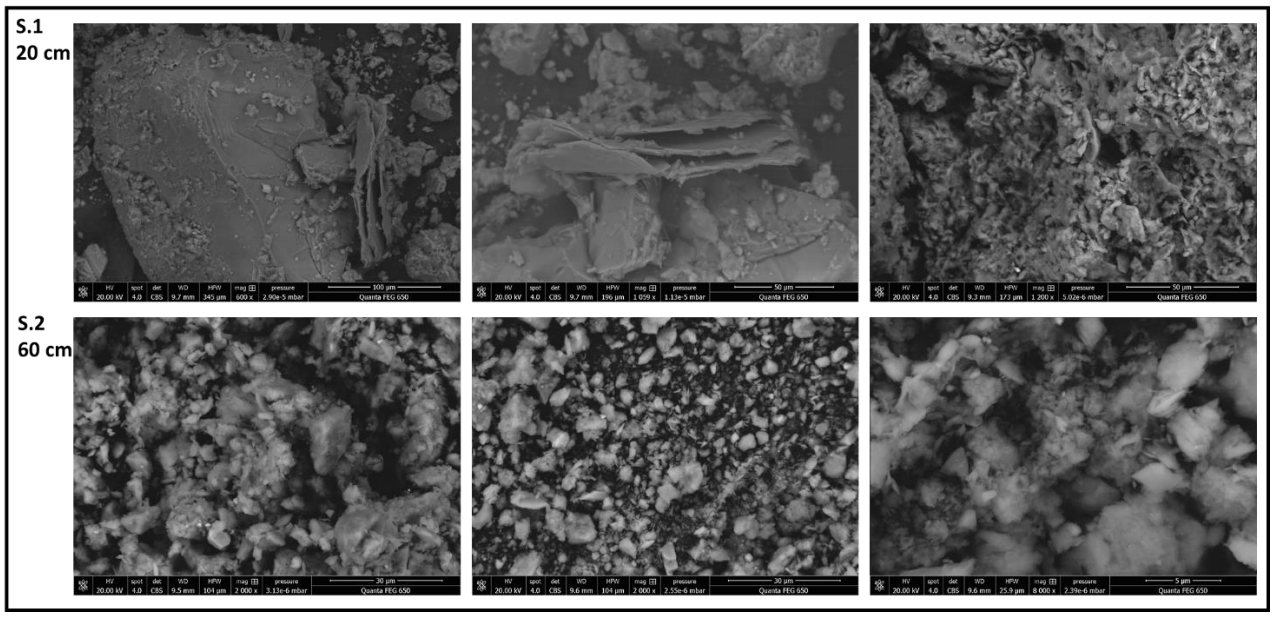

Figure 4. Representative mineralogical analysis using scanning electron microscopy backscatter and secondary electron imagery projections of Twin Ma sample 1 (20 cm) and 2 (60 cm).

Scanning electron microscopy SEI analysis revealed mineral structure dominated by fine quartz grains and layered clay mineral structures (Fig. 4). Sample 1 (20 cm depth) possessed a larger quantity of coarser quartz grains (>300 µm) than were visible in sample 2 (60 cm depth), dominated by grain sizes <10 µm. X-ray microanalysis mapping showed both sample elemental spectra to be dominated by the silica, oxygen and aluminium with very little calcium presence in the samples reflecting a lack of calcium carbonate crystals in the core (Fig. 5). Specific analysis of Ca and Na evidenced localised areas of enrichment in small micro pockets, however no evidence of authigenic mineral precipitation was found in Twin Ma Lake.

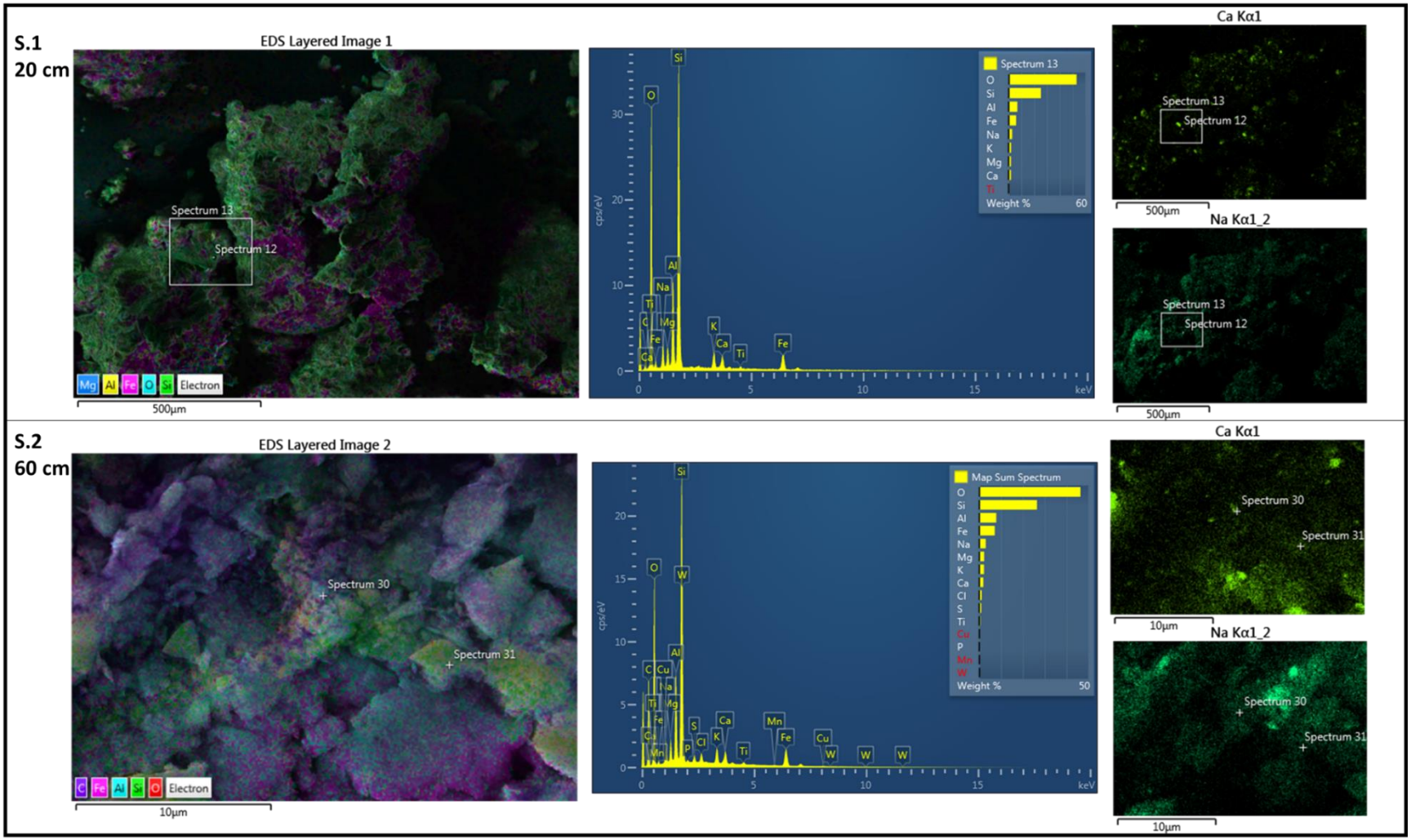

Figure 5. Representative X-ray microanalysis mapping on Twin Ma sediment samples 1 (20 cm) and 2 (60 cm), with accompanying elemental spectra showing mineral composition and area mapping of Ca and Na concentration.

4.3. Taung Pyauk biomarker results

4.3.1. Taung Pyauk *n*-alkane distribution

Taung Pyauk provided a ~ 1500-year record of *n*-alkane distribution. Mean CPI was 10.1 (min = 3.4 max = 26), exhibiting a prevailing odd over even dominance (Fig. 6). Odd chain length predominance was highest in longer chain lengths, reducing significantly at lower chain lengths (C_{17}–C_{22}). The proportion of long chain (C_{27}–C_{35}) *n*-alkanes contributed between 61% and 91% to the total *n*-alkane (C_{17}-C_{40}) concentration. Total *n*-alkane concentration (∑ (C_{17} – C_{40})) ranged from 1.3 to 14.7 µg g^{-1} sediment (sed) with depth, with pronounced enrichment (~ 1700, 1350, 1200, 1050, 700 (AD)) and depletion (~ 1900, 750, < 600).

Long chain dominance was reflected by a mean ACL of 29.2 (min = 28.4, max = 29.9) with C31 being the overall dominant homologue with the highest summed concentration (∑ (core) = 134.8 µg g^{-1} sed). Mid chain *n*-alkanes (C_{21}-C_{26}) were depleted relative to their long chain counterparts, contributing between 8.9% and 35% to the total *n*-alkane concentration with depth. The most enriched and variable medium chain homologue was C_{23}, having a summed concentration of 48.7 µg g^{-1} sed within the total core and a peak concentration of 1.49 µg g^{-1} sed (Table. 3). Short chain homologues (C_{17} – C_{20}) were marginally dominated by C_{19}, though a low preference for odd chain lengths was exhibited overall (Fig. 6). The average pattern showed an enrichment of short chain lengths < C_{21} compared to highly depleted C_{21}.

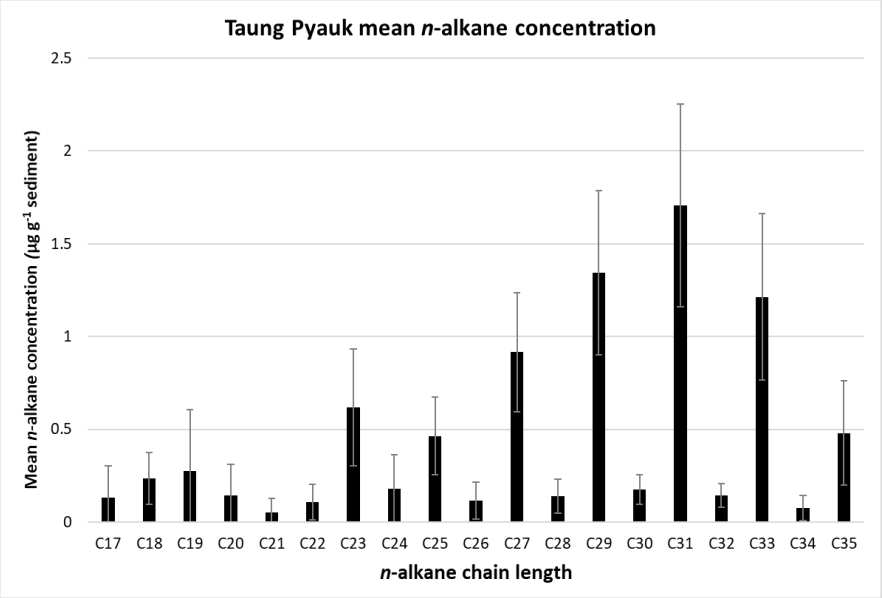

Figure 6. Taung Pyauk sediment core mean n-alkane concentration for each homologue length. Error bars display 1 positive and negative standard deviation.

Table 3. Taung Pyauk n-alkane homologues and indices summary statistics.

	N	Min	Max	Sum	Mean	Stand. dev	Median
Paq	79	0.12	0.43	-	0.26	0.07	0.27
ACL	79	28.42	29.90	-	29.15	0.33	29.17
CPI	79	3.37	27.62	-	10.13	4.38	9.71
Medium chain %	79	8.88	34.97	-	19.40	5.79	19.28
Long chain %	79	65.03	91.12	-	80.60	5.79	80.72
Total n-alkanes ug g^{-1} sed	79	1.32	17.14	-	8.58	2.96	8.77
C_{17} (ug g^{-1} sed)	79	0.00	0.83	10.23	0.13	0.17	0.07
C_{18} (ug g^{-1} sed)	79	0.00	0.75	18.59	0.24	0.14	0.22
C_{19} (ug g^{-1} sed)	79	0.02	1.81	21.57	0.27	0.33	0.15
C_{20} (ug g^{-1} sed)	79	0.02	1.04	11.25	0.14	0.17	0.09
C_{21} (ug g^{-1} sed)	79	0.00	0.46	4.11	0.05	0.07	0.03
C_{22} (ug g^{-1} sed)	79	0.01	0.48	8.50	0.11	0.10	0.08
C_{23} (ug g^{-1} sed)	79	0.05	1.49	48.70	0.62	0.32	0.60
C_{24} (ug g^{-1} sed)	79	0.00	0.90	14.00	0.18	0.19	0.14
C_{25} (ug g^{-1} sed)	79	0.07	1.13	36.67	0.46	0.21	0.47
C_{26} (ug g^{-1} sed)	79	0.01	0.55	9.06	0.11	0.10	0.10
C_{27} (ug g^{-1} sed)	79	0.10	1.63	72.31	0.92	0.32	0.93
C_{28} (ug g^{-1} sed)	79	0.01	0.41	10.98	0.14	0.09	0.14
C_{29} (ug g^{-1} sed)	79	0.17	2.42	106.06	1.34	0.44	1.31
C_{30} (ug g^{-1} sed)	79	0.01	0.40	13.70	0.17	0.08	0.16
C_{31} (ug g^{-1} sed)	79	0.27	3.09	134.81	1.71	0.55	1.73
C_{32} (ug g^{-1} sed)	79	0.01	0.30	11.32	0.14	0.07	0.14
C_{33} (ug g^{-1} sed)	79	0.18	2.32	95.82	1.21	0.45	1.18
C_{34} (ug g^{-1} sed)	79	0.00	0.32	6.00	0.08	0.07	0.05
C_{35} (ug g^{-1} sed)	79	0.00	1.34	37.88	0.48	0.28	0.42

4.3.2. Taung Pyauk *n*-alkane homologue and indices change

Taung Pyauk *n*-alkane indices all displayed sharp oscillation throughout the core length reflecting distinct perturbations in chain length distribution on decadal to centurial timescales throughout the ~ 1500-year record (Fig. 8). A relative period of lower CPI and ACL values occurred between 2000 - 1600, followed by maximum values between 1600 - 1400 and middle range values prior to 1200. Taung Pyauk CPI had a significant positive Spearman's correlation with ACL (Spearman's correlation (r_s) = 0.35, n = 79; $p < 0.01$), and correspondingly a negative correlation with Paq (r_s = - 0.45, n = 79; $p < 0.01$). Peaks illustrating this relationship were present around years 1600, 1400, 1200 and 800, although the relationship was not always distinctly clear (i.e. ~ 1800), evidencing some variability.

Both Paq and C_{23} were closely correlated (Pearson's correlation (r) = 0.74, n = 79; $p < 0.01$) with C_{23} accounting for 55% of variation in Paq (R^2 = 0.55), thus constituting the defining medium chain component of Paq formulation relative to C_{25} (R^2 = 0.26). Total *n*-alkane concentration showed no overall significant negative correlation with ACL (r_s = - 0.12, n = 79; $p > 0.1$) or CPI (r_s = - 0.17, n = 79; $p > 0.1$), but some qualitative evidence of an inverse relationship between CPI/ACL with total *n*-alkane concentration was seen during pronounced fluctuations (i.e. ~ 1500, 1400, 800).

Short chain *n*-alkane fluctuations were most evident in C_{19} and C_{17}**,** however the overall concentration difference between odd and even chain lengths were small (Fig. 7). A closely matching trend in all short chain *n*-alkanes was present, with different magnitudes of change (C_{19} > C_{17} > C_{18} > C_{20} > C_{21}). Roughly 8 localised peaks in C_{19} were distinguished; 4 of which exceeded a concentration of 1 µg g^{-1} sed at their respective age (650, 1050, 1850, 1990) and were mimicked by less pronounced increases in C_{17} in addition to peaks in total *n*-alkane concentration.

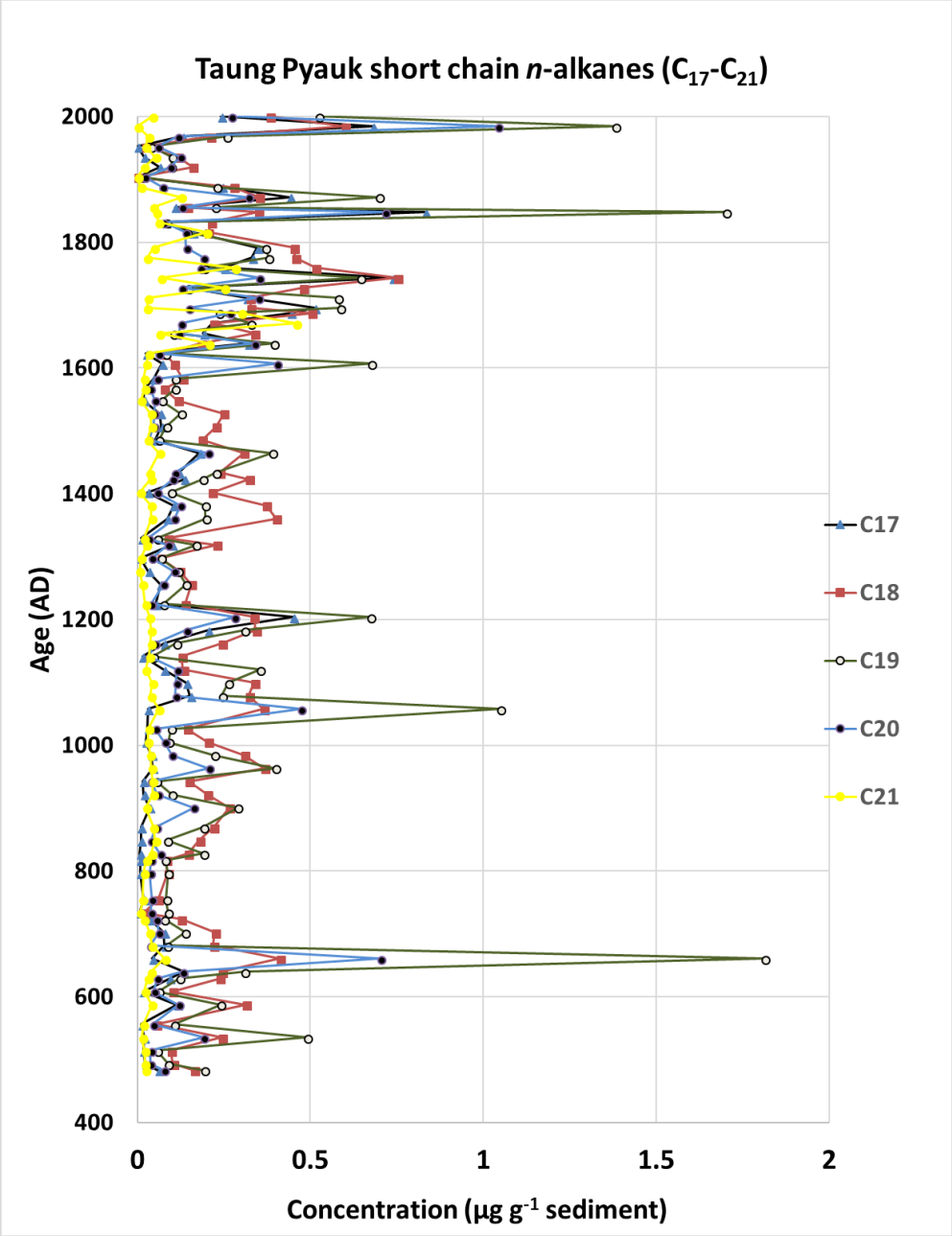

Figure 7. Short chain (C_{17} - C_{21}) n-alkane concentration with depth throughout the radiocarbon dated Taung Pyauk core.

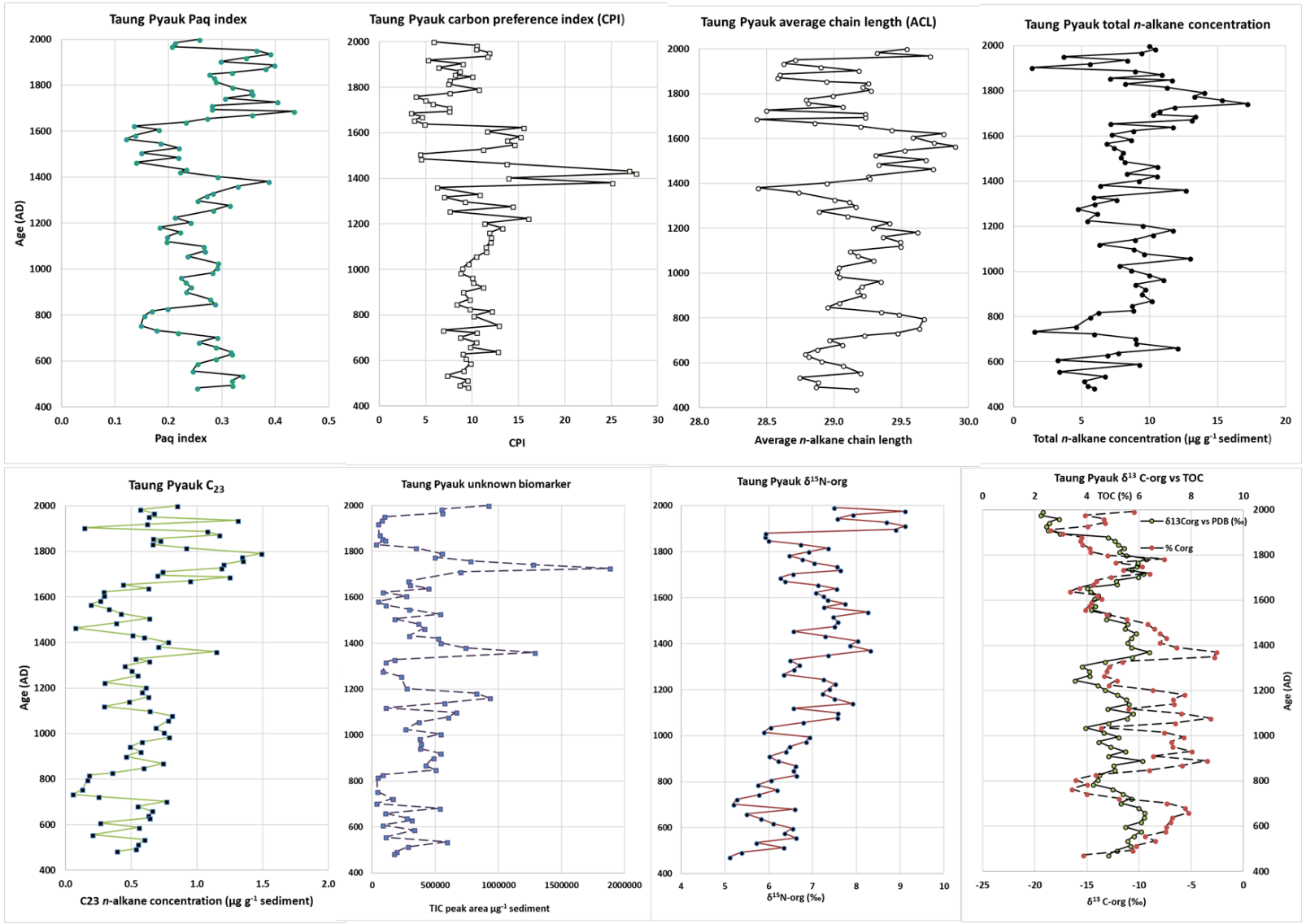

Figure 8. Taung Pyauk multiple n-alkane indices, stable isotope and biomarker results compilation over a 1500-year time series.

4.3.3. Taung Pyauk bulk organic matter $\delta^{13}C$, $\delta^{15}N$, TOC and further biomarker analysis

Taung Pyauk bulk OM $\delta^{13}C$ ($\delta^{13}C_{TOC}$) contained a mean $\delta^{13}C$ value of -12.7 ‰, ranging from -19.5 to - 9.1 ‰ at around years 2000 and 1400, respectively. Mean total organic carbon (TOC) content was 5.7 %, ranging from 2.6 % to 9 % around 1850 and 1350. Both TOC and $\delta^{13}C_{TOC}$ significantly correlated (r_s = 0.62, n = 79; p < 0.01) showing distinctive coinciding maxima. The most sustained TOC and $\delta^{13}C_{TOC}$ increase occurred from roughly 800 to 1200 (Fig. 8). An exception to the close correlation occurred post 1900 when noticeable divergence between TOC and $\delta^{13}C$ was evident. Peaks in $\delta^{13}C$ and TOC corresponded reasonably well to increased Paq C23 *n*-alkane concentration (i.e. ~ 1700, 1400, 600) and hence some inverse relationship with ACL and CPI was visible (i.e. ~ 1600, 1400, 750).

Bulk OM $\delta^{15}N$ ($\delta^{15}N_{TOC}$) varied between 5.1 and 9.1 ‰ reflecting an overall ^{15}N depletion (Fig. 8). An insignificant negative correlation was present between $\delta^{15}N_{TOC}$ and $\delta^{13}C_{TOC}$ (r_s = 0.2, n = 79; p < 0.1), however the relationship was not distinctively clear as clear periods of $\delta^{15}N$ enrichment or depletion were lacking.

A compound (biomarker X) was found and quantified in 71 of 79 samples and displayed higher TIC peak areas per sample weight around years 1500, 1350, 1150 (Fig. 8). A mass/charge ratio of 552 suggested a chemical formula $C_{40}H_{72}$ with a characteristic m/z peak at 123. Compound peak occurrences corresponded with peaks in bulk $\delta^{13}C$, TOC, C_{23} *n*-alkane concentration and inversely with *n*-alkane CPI values. Unresolved complex mixture (UCM) was prevalent in Taung Pyauk between 1600 and 1800 (Appendix. 6), corresponding to a period of low CPI values (Fig. 8).

4.4. Twin Ma high temporal resolution biomarker results

4.4.1. Twin Ma *n*-alkane distribution

Twin Ma 100-year sediment record *n*-alkane abundance resembled a bimodal distribution dominated by long and medium length homologues (Fig. 9). Carbon preference index illustrated an odd over even preference throughout, however a lower odd *n*-alkane homologue predominance ($\bar{x}$ = 8.1, min = 2.9, max = 10.7) than Taung Pyauk was evident (Fig. 9; Table. 4). Like Taung Pyauk, long chain *n*-alkanes (C_{27}-C_{33}) dominated throughout the core (Fig. 9), contributing between 63.8 % and 85.2 % to the total abundance. Mean total *n*-alkane abundance (C_{17}–C_{40}) per sample was 6.5 µg g^{-1} sed, ranging between 1.8 and 20.1 µg g^{-1} sed at 16 cm and 28 cm depths respectively.

Twin Ma mean ACL (28.9) was lower than Taung Pyauk (29.2) but still reflected a long chain (>C_{27}) dominance; with C_{33} as the mean dominant *n*-alkane homologue. Twin Ma average mid-chain *n*-alkane (C_{21}-C_{26}) composition was 25.9 % and ranged from 14.8 % to 36.3 %, reflecting a higher relative contribution of C_{23} and C_{25} compared to Taung Pyauk (Fig. 6 & 9). Total short chain homologues (∑ (C_{17} - C_{20}) were present in lower average concentration (0.52 µg g^{-1} sed) than Taung Pyauk, but with a matching trend of low odd over even preference and an overall dominance of C_{19}.

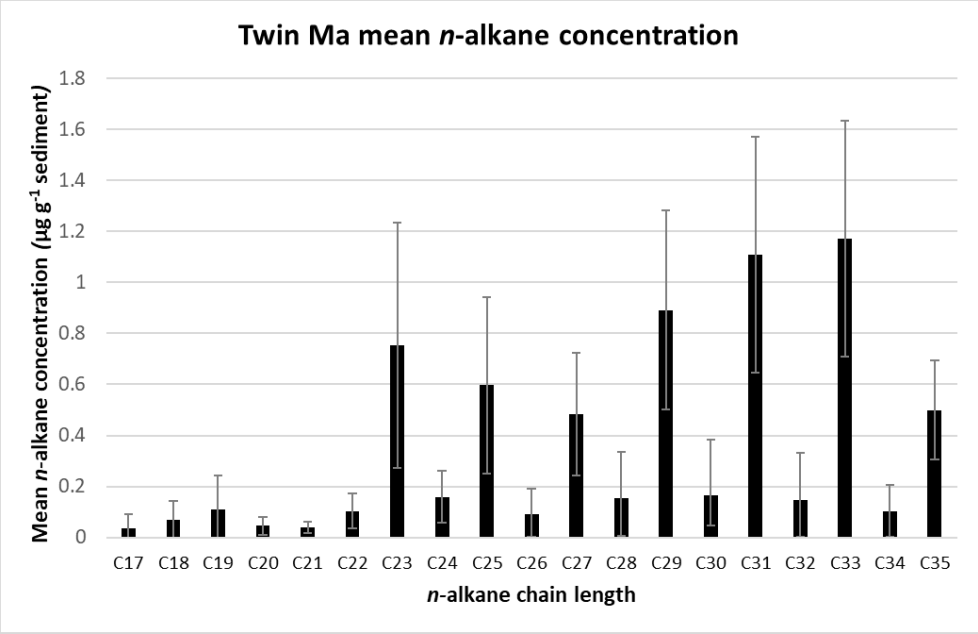

Figure 9. Twin Ma sediment core mean n-alkane concentration for each homologue length. Error bars display 1 positive and negative standard deviation.

Table 4. Twin Ma n-alkane homologues and indices summary statistics.

	N	Min	Max	Sum	Mean	Stand. dev	Median
Paq	36	0.20	0.48	-	0.36	0.07	0.36
ACL	36	28.10	29.85	-	28.90	0.44	28.90
CPI	36	2.87	10.66	-	8.08	1.79	8.46
Medium chain %	36	14.84	36.25	-	25.92	5.30	25.71
Long chain %	36	63.75	85.16	-	74.08	5.30	74.29
Total n-alkanes ug g^{-1} sed	36	1.84	20.27	-	6.79	3.41	6.13
C_{17} (ug g^{-1} sed)	36	0	0.24	1.26	0.04	0.06	0.02
C_{18} (ug g^{-1} sed)	36	0	0.37	2.44	0.07	0.08	0.05
C_{19} (ug g^{-1} sed)	36	0	0.56	3.97	0.11	0.13	0.07
C_{20} (ug g^{-1} sed)	36	0	0.15	1.61	0.04	0.04	0.03
C_{21} (ug g^{-1} sed)	36	0.01	0.12	1.39	0.04	0.02	0.03
C_{22} (ug g^{-1} sed)	36	0.02	0.28	3.73	0.10	0.07	0.08
C_{23} (ug g^{-1} sed)	36	0.15	2.02	27.13	0.75	0.48	0.64
C_{24} (ug g^{-1} sed)	36	0.04	0.56	5.70	0.16	0.10	0.13
C_{25} (ug g^{-1} sed)	36	0.17	1.96	21.50	0.60	0.35	0.52
C_{26} (ug g^{-1} sed)	36	0.03	0.63	3.33	0.09	0.10	0.07
C_{27} (ug g^{-1} sed)	36	0.14	1.40	17.45	0.48	0.24	0.44
C_{28} (ug g^{-1} sed)	36	0.05	1.15	5.60	0.16	0.18	0.13
C_{29} (ug g^{-1} sed)	36	0.24	2.41	32.09	0.89	0.39	0.92
C_{30} (ug g^{-1} sed)	36	0.03	1.39	5.94	0.17	0.22	0.13
C_{31} (ug g^{-1} sed)	36	0.32	2.88	39.93	1.11	0.46	1.06
C_{32} (ug g^{-1} sed)	36	0.04	1.18	5.21	0.14	0.19	0.12
C_{33} (ug g^{-1} sed)	36	0.25	2.15	42.25	1.17	0.46	1.15
C_{34} (ug g^{-1} sed)	36	0.02	0.65	3.67	0.10	0.10	0.08
C_{35} (ug g^{-1} sed)	36	0.10	0.92	18.00	0.50	0.19	0.50

4.4.2. Twin Ma *n*-alkane homologue and indices change

Twin Ma indices of *n*-alkane abundance distribution showed distinct periods of change over established the 100-year extent; evidencing 4 periods of relatively increased short chain *n*-alkane input (lower ACL) around roughly 2005, 1990, 1965 and 1925 (Fig. 11). Average chain length fluctuated highly with a general trend of increasing ACL minima towards the present day. No overall statistical correlation was present between CPI and ACL profiles (r_s = 0.03, n = 36; p > 0.1), or CPI and Paq (r_s = - 0.04, n = 36; p > 0.1). However, most CPI minima loosely corresponded with periods of lower ACL and higher Paq values.

Changes in C_{23} explained 55 % of variance in the Paq index (R^2 = 0.55) whereas 37 % was explained by C_{25}. Thus, C_{23} constituted primary input chain length of the Paq index, as in Taung Pyauk (Fig. 8 & 11). Total *n*-alkane and C_{23} profiles closely matched, exhibiting significant peaks around 1925 and 1975. Total *n*-alkane concentration correlated negatively with ACL (r = - 0.38, n = 36; p < 0.05) and CPI (r = - 0.38, n = 36; p < 0.05), a relationship visible is Taung Pyauk but without statistical significance.

Twin Ma short chain *n*-alkanes possessed a similar trend in fluctuation with depth but a higher relative even chain homologue dominance to Taung Pyauk (C_{19} > C_{18} > C_{20} > C_{17} > C_{21}). Five visible periods of C_{19} enrichment were visible between roughly 1915 and 1965, the most pronounced of which occurring around 1925. Short chain homologues less abundant post 1965 and displayed little significant fluctuation.

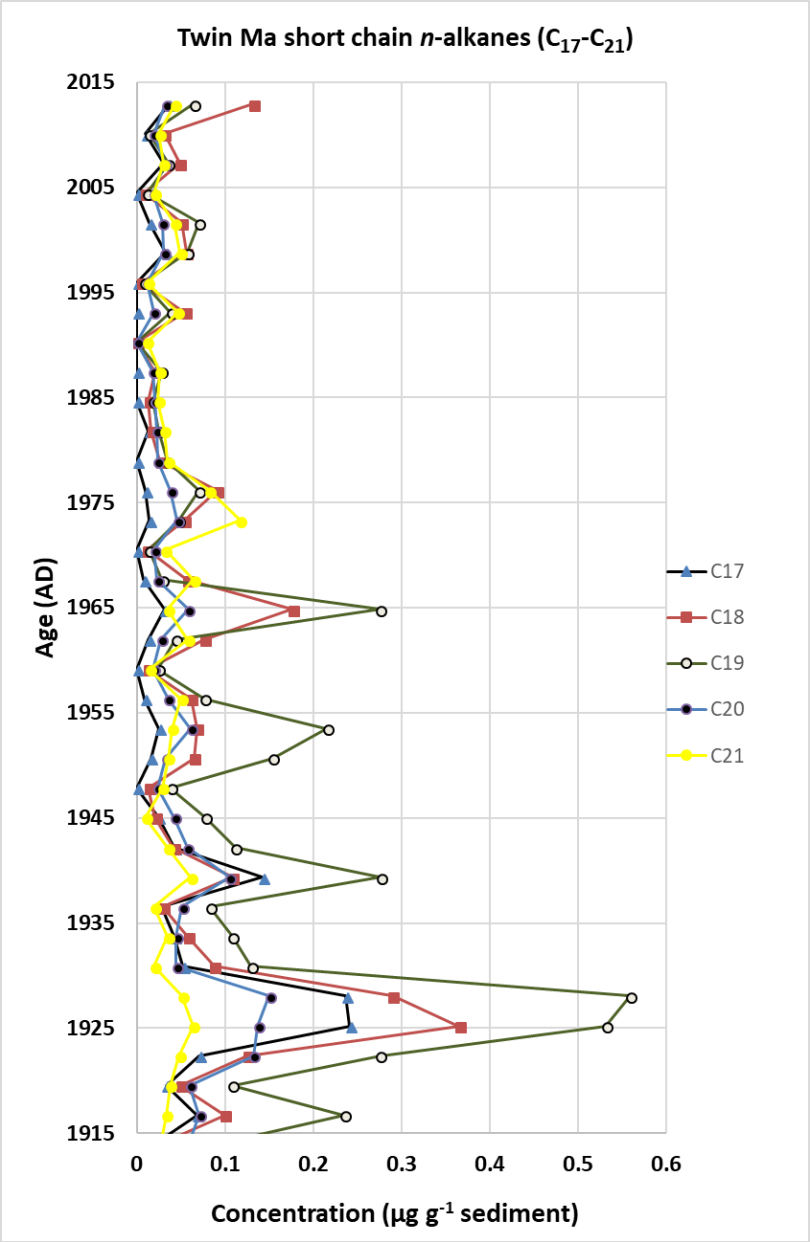

Figure 10. Short chain (C_{17} - C_{21}) n-alkane concentration with depth throughout the radiocarbon dated Twin Ma core.

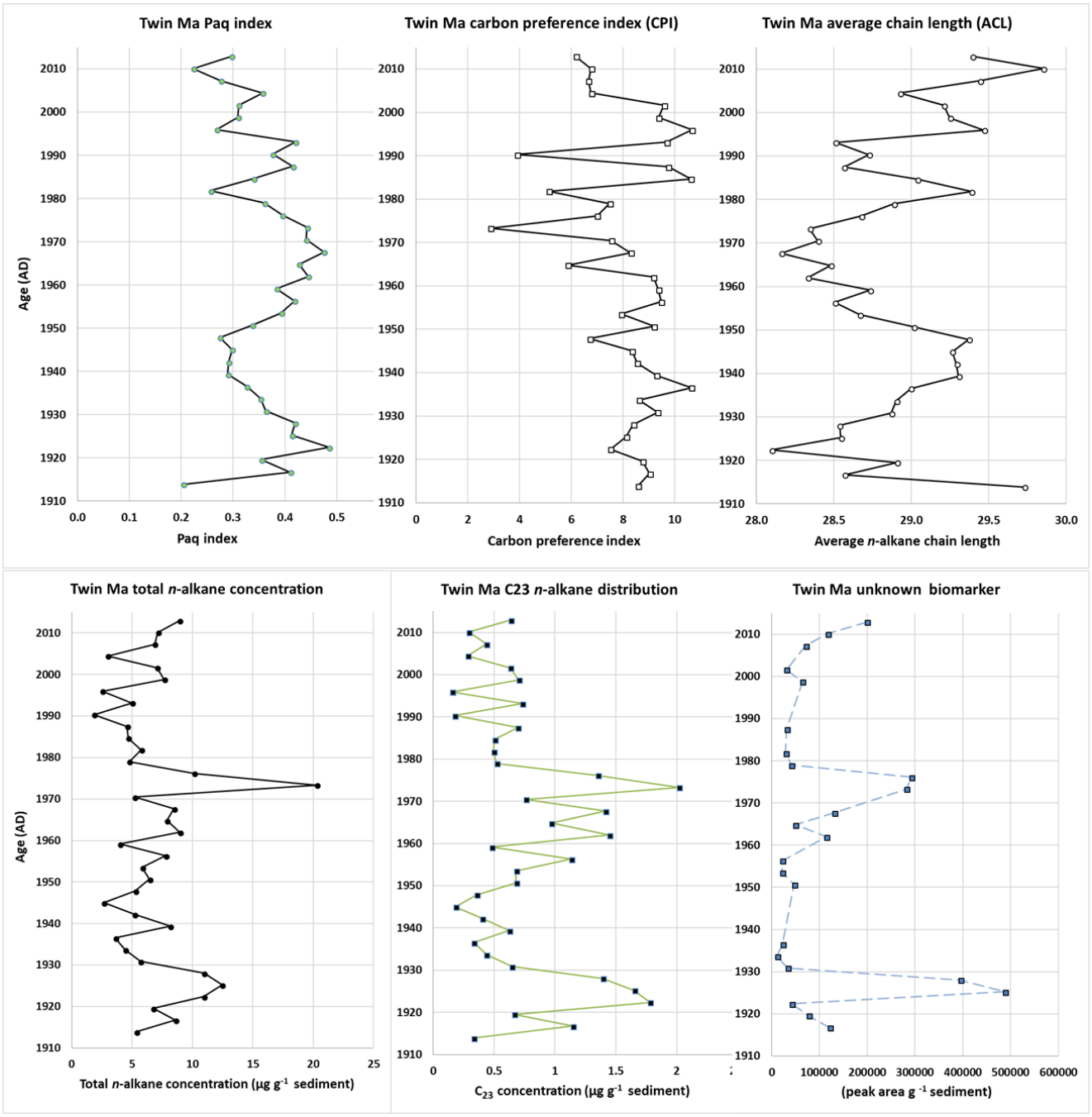

Figure 11. Twin Ma n-alkane multiple indices and stable isotope results compilation over the chronological 100-year time series.

4.4.3. Twin Ma further biomarkers and unresolved complex mixture

Like Taung Pyauk, a biomarker with 552 m/z total mass and 123 m/z characteristic peak (biomarker x) displayed 2 significant peaks in Twin Ma, occurring roughly around years 1925 and 1975. Enrichment coincided with minima in ACL and maxima in both total *n*-alkane (C_{17}-C_{40}) and C_{23} concentration (Fig. 11). The correlation between compound peak area and total *n*-alkane concentration was statistically significant (r_S = 0.77, n = 24; $p < 0.001$) indicating strong covariance. The compound peak area also showed significant negative correlation with CPI (r_S = - 0.39, n = 24; $p < 0.05$), distinguishable around 1975. Unresolved complex matrix was intermittently prevalent throughout the Twin Ma record and typically occurred at lower retention times alongside short-chain *n*-alkanes.

4.4.4. Twin Ma *n*-alkane distribution climate dependence

Comparison of *n*-alkane indices with a post 1901 observational climate record revealed climate related trend *n*-alkane indices. Mean air temperature over 3-year combined periods correlated positively with ACL (r = 0.56, n = 36; $p < 0.01$) and negatively with C_{23} concentration (r = - 0.41, n = 36; $p < 0.05$) (Fig. 12). Regression analysis showed proportionate increase between air temperature and ACL increase; inferring a *n*-alkane ACL increase of 1 per °C increase in mean air temperature.

No significantly clear trend was evident between precipitation patterns and *n*-alkane distribution suggesting precipitation patterns poorly explain *n*-alkane variability. Carbon preference index correlated negatively with the number of months over the corresponding 3-year period with < 20 mm precipitation (r_S = - 0.32, n = 36; $p < 0.05$). However, overall variability in CPI was poorly explained and the relationship was not distinctively clear.

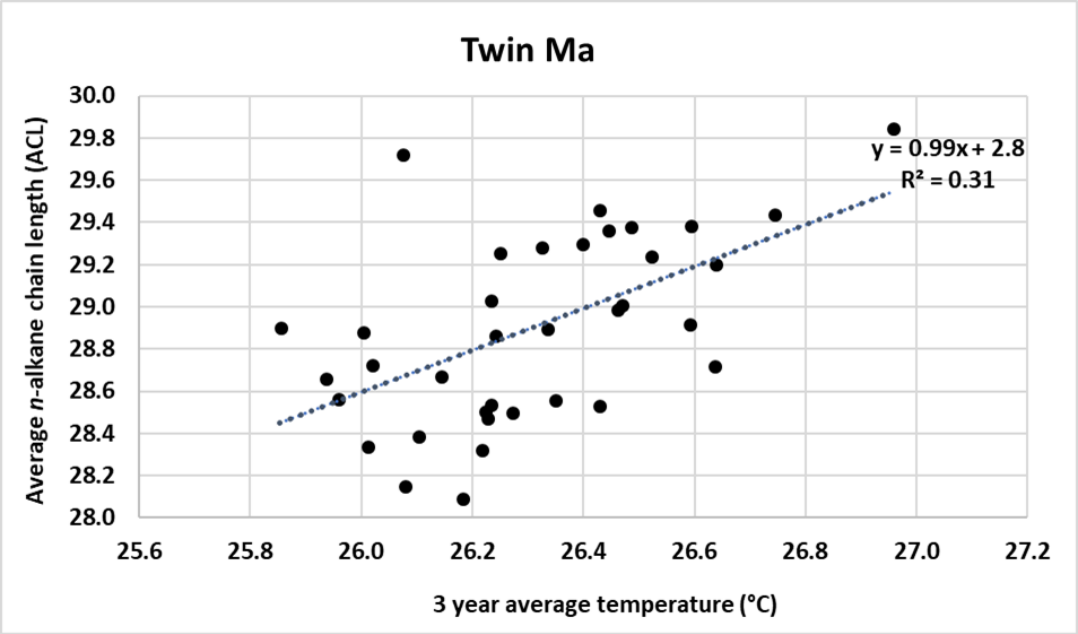

Figure 12. Biplot of Twin Ma ACL and compiled 3-year average air temperature over the representative area.

5. Discussion

5.1. Twin Ma mineral composition and stratigraphy

Analysis of Twin Ma mineral composition and stratigraphy was undertaken to characterise possible inorganic sediment change from lithogenic to authigenic during wet and dry seasons respectively (Sun et al., 2016). Little visible change was evident throughout the Twin Ma sedimentary archive suggesting a relatively uniform depositional environment during 100-year recorded time-span. A richness of reduced S species was indicative of a reducing, euxinic sediment column with anoxia throughout (Morse et al., 1987). Mineralogical analysis revealed a lithogenic fine-grained silicate and aluminosilicate composition, demonstrating low energy deposition of weathered minerals sourced from the surrounding volcanic geology. No calcium carbonate mineral formation was evident within the core; a distinct contrast to the laminated $CaCO_3$ layers revealed by Sun et al., (2016) in the nearby Twintuang crater lake that were attributed to strong dry season evaporation and *Spirulina* blooms. The precipitation of $CaCO_3$ has long been understood as a function of the saturation (Ω) of the parent solution (Cloud, 1962).

Carbonate ions are considered the dominant inorganic carbonate species in Twin Ma given the high recorded pH (10 -11), therefore an absence of $CaCO_3$ precipitates is likely explained by a lack of free Ca^{2+} ions, dissolution related to unfavorable sedimentary physicochemical conditions, or inhibition of nucleation by other substances.

5.2. Interpretation of *n*-alkane proxies and biomarkers in Twin Ma and Taung Pyauk

Molecular distribution of *n*-alkanes has been frequently used to discern changes in OM sources across varying environmental gradients and temporal frames (Ortiz et al., 2013; Sun et al., 2013; Mead et al., 2005; Zech et al., 2013; Zhang et al., 2017). Combining results from both crater lakes gave a high resolution 100-year record (Twin Ma) and an extended 1500-year record (Taung Pyauk) of OM input variation. Both cores possessed high frequency oscillation with some evidence signals of longer pronounced fluctuations in *n*-alkane composition; reflecting difference in chain length distribution and the overall odd over even chain length preference (Fig. 8 & 11). The dominance of C_{31} and C_{33} homologues in Taung Pyauk and Twin Ma respectively, implies a consensus that xerophytic C_4 grasses or vascular land plants are the principal *n*-alkane source from hydrological input within the catchment or aeolian transport from the regional area (Freeman and Pancost, 2014; Vogts et al., 2012). The natural affinity of terrestrial vegetation for both higher ACL and CPI values in terrestrial plant biosynthetic pathways was statistically evident in Taung Pyauk (r_s = 0.35, n = 79; $p < 0.01$) with CPI peaks coinciding with ACL maxima (Eglinton and Hamilton, 1967). This covariance of ACL and CPI was not statistically evident in Twin Ma. However, the lowest CPI values were noticeably coupled to ACL minima around 1925 and 1975 (Fig. 11).

Closed crater lake systems provide a unique environment to investigate environmentally instigated shifts in vegetation contribution when the characteristic n-alkane suite of the major OM input sources is known (Sun et al., 2013). Total *n*-alkane homologue (C_{17}-C_{40}) concentration in Twin Ma had a significant negative correlation with ACL and CPI; implying that OM sources with a characteristically less terrestrial identity (lower ACL and CPI) are the primary contributors during periods of high OM input. Increase in C_{17}-C_{25} concentration generally typifies organism shifts

within a lacustrine environment to an algal (C_{17}-C_{21}) and submerged/floating aquatic macrophyte (C_{23}-C_{27}) dominated system (Sun et al., 2013; Ficken et al., 2000). In both crater lakes, C_{19} (cyanobacteria) and C_{23} (submerged/floating macrophytes) were the most characteristic short and mid chain homologues respectively, suggesting fluctuation in these homologues typify OM source change (Ortiz et al., 2013). Moreover, the distinctively low odd over even preference in short chain (C_{17}-C_{20}) *n*-alkanes provides further evidence for a decayed cyanobacterial origin (Cranwell et al., 1987).

Notable ambiguity remains regarding the use of *n*-alkane indices as a precise source organism indicator due to region specific and taxonomical variation in *n*-alkane (Freeman and Pancost, 2014). In the case of Twin Ma and Taung Pyauk; observational evidence may support that in the absence of abundant visible macrophytes, the intensity of dry season blooms of *Spirulina* and other algae play a decisive role in increasing short chain *n*-alkane (C_{21} and C_{23}) concentration and consequently overall *n*-alkane (organic matter) richness.

A suite of biomarkers was identified and quantified in both lakes however due to time constraints only one was analysed throughout the core and presented in this study (Appendix. 3). According to RH Smittenberg (2018, personal communication), most identified lipid compounds were ring-A degraded triterpenoids indicative of hydrogen sulphide rich sediment in which electron donation by inorganic sulphide species can induce non-biological reduction of OM. Such reactions have evidenced occurrences during early diagenesis (Hebting, 2006). Furthermore, most samples in both lake sediment cores contained a set of nearly identical compounds with a m/z 552 nominal mass and a 123 m/z base peak, suggesting these compounds are structural isomers of saturated C_{40} isoprenoid compounds produced by anoxygenic sulphur bacteria (Appendix. 3). However, observed mass spectra did not correspond to a known saturated biomarker version of photosynthetic sulphur bacteria (usually containing an aryl group: (β/iso)-renieratene chlorobactene or okenone). Neither did they correspond to other known saturated carotenoids (e.g. β-carotane). In both lakes, the exhibited shallow chemocline with accompanying photic zone euxinia. Consequently, these biomarkers may be products of photic zone penetration by anoxygenic sulphur bacteria that were degradative products of the aforementioned hydrogen sulphide-mediated reduction (RH Smittenberg, personal communication, 2018; Sinninghe Damsté, 1993; Brocks et al, 2005). The unknown analysed biomarker (biomarker x) strongly covaried with C_{23}, total *n*-alkane concentration and $\delta^{13}C_{TOC}$ (Fig. 8 & 11). Enrichment of this

compound is presumably associated with shifts in lake trophic status, produced by increasing productivity by photosynthetic organisms above (oxygenic) or below (anoxygenic) the chemocline. Therefore, biomarker x enrichment is potentially indicative of physical stratification intensity or level of oxygen consumption. Further research and classification of these biomarkers beyond this study is required to fully understand their source and environmental implications in both crater lakes.

The occurrences of UCM in both lake sediments alongside comparatively reduced CPI values may indicate enhanced microbial degradation in anoxic sediments or oil contamination (Miralles et al., 2007). The small crater catchments and long temporal record of UCM makes an exclusive anthropogenic oil source unlikely. The cyclic and branched alkane composition of UCM is microbially resistant and typically remains after microbial breakdown of short chain *n*-alkanes (Miralles et al., 2007). Anaerobic chemotrophic and phototrophic (anoxygenic) pathways of alkane breakdown are possible using nitrate, sulphate and iron as recognized substrates (Widdel and Rabbus, 2001). Occurrence of UCM potentially indicates intense episodic microbial hydrocarbon degradation beneath the oxic/anoxic chemocline boundary during periods of short and medium *n*-alkanes enrichment (high autochthonous OM production).

5.3. Source attribution of bulk organic matter $\delta^{13}C$, $\delta^{15}N$ and TOC change in Taung Pyauk

Isotopic composition of bulk OM can imply shifts in species composition and/or changing environmental conditions (i.e. temperature, salinity, CO_2 concentration) within a limnic system through the magnitude enrichment or depletion of stable heavy isotopes (i.e. $\delta^{13}C$, $\delta^{15}N$) (Liu et al., 2013; Freeman and Pancost., 2014). Lake Taung Pyauk demonstrated a closely linked relationship between $\delta^{13}C_{TOC}$ and TOC; having distinctly less negative $\delta^{13}C$ values as TOC increased. Studies by Neumann et al., (2002) combined positive shifts in $\delta^{13}C_{TOC}$ with observations of eutrophication to imply increased algal photosynthetic activity. Taung Pyauk $\delta^{13}C_{TOC}$ ranged between - 9.1 ‰ and -19.5 ‰; mostly inside the observed range for aquatic C_3 plants (− 22‰ to − 12‰) but suggesting some input from isotopically heavier C_4 vegetation within the catchment. Accordingly, shifts in trophic state are implied by distinctly higher $\delta^{13}C_{TOC}$, Paq,

C_{23} and *n*-alkane concentration (i.e. 1800, 1400), in addition to some visible inverse relationship with CPI and ACL.

Accompaniment of higher $\delta^{13}C_{TOC}$ and TOC values with greater short and medium chain n-alkane concentration (C_{23} along with C_{19}) and lower CPI values provide a reliable indicator that cyanobacterial bloom conditions cause dramatic OM enrichment. Isotopic shifts to heavier fractions in phytoplankton are encountered with increased cell growth rate, size and membrane permeability (Rau et al., 1997). Transition to higher $\delta^{13}C_{TOC}$ is attributable to a source change to aquatic C_3 primary producers utilising isotopically heavier ($\delta^{13}C = \sim 0$ ‰) bicarbonate ions as a carbon source in the alkaline lake, as opposed to CO_2 ($\delta^{13}C = \sim$ -7 ‰) (Bianchi and Canuel., 2011). Furthermore, a reduction in pCO_2 reduces the discrimination against ^{13}C in the enzymatic carbon fixation pathway and limits isotopic fractionation almost exclusively to the less pronounced cellular diffusion phase (Chikaraishi., 2014). Environmentally induced $\delta^{13}C$ increase in Tuang Pyauk can be accounted for by a combination of decreasing CO_2 solubility at higher waterbody temperatures and productivity-driven CO_2 consumption within a limited carbon pool; both indicative of an intense dry season (Neumann et al., 2002).

$\delta^{15}N_{TOC}$ has been applied across different environments as a tracer to distinguish large scale changes in biochemical fixation pathways through differences in ^{15}N discrimination (Robinson, 2001). Taung Pyauk $\delta^{15}N_{TOC}$ signal was more complex than $\delta^{13}C_{TOC}$, exhibiting high frequency fluctuation within a range of 4 ‰. A statistically insignificant negative relationship occurred between $\delta^{15}N_{TOC}$ and $\delta^{13}C_{TOC}$, weakly suggesting that increased $\delta^{13}C$ accompany lower $\delta^{15}N$ values. However, the complexity of the N cycle and makes a clear pattern difficult to discern. Soda lakes are identified as microbially rich environments containing all functioning groups of microbe metabolites with complex microbial food webs with simultaneous ^{15}N fractionations (Paul Anthony et al., 2012). Some visible fluctuation to lower $\delta^{15}N_{TOC}$ occurred roughly around peaks in $\delta^{13}C_{TOC}$ and TOC. Such occurrences have been evidenced in highly productive systems where isotopically light N^2 fixation by cyanobacteria compensates for a lack of bioavailable N species or the discrimination against ^{15}N is reduced during periods of nitrate limitation (Neumann et al., 2012).

5.4. Climatic signals and environmental change inferred from Twin Ma and Taung Pyauk geochemical record

5.4.1. Interpretation of modern day climatic trend in Twin Ma

Comparison of a climatic data set with the chain-length distribution of *n*-alkanes (ACL) in Twin Ma displayed a relatively pronounced low frequency climatic signal over 100 years; evidencing a nearly linear increase with mean annual air temperature over a combined 3-year resolution. Results suggest; i) a biosynthetically mediated increase in the ACL of *n*-alkane waxes residing on the stomata in response to increased air temperature and aridity, ii) vegetational species compositional change within the crater catchment to C_4 or higher plant species, iii) selective microbial attack of shorter chain homologues increasing *n*-alkane ACL.

Bush and McInerney, (2015) used a longitudinal transect in the US to evidence soil *n*-alkane ACL increase with growing season temperature, suggesting soil constitutes an integrated average of *n*-alkane distribution without interspecies genetical variation as individual plants do. Furthermore, their study found region specific C_4 plant abundance did not correlate significantly with ACL, suggesting that over decadal timescales changes from C_3 to C_4 vegetation may have negligible impact on ACL. These observations imply a biosynthetic origin to synthesize longer, more hydrophobic molecules capable of better restricting stomatal water loss in arid conditions (Bush and McInerney, 2015). This trend may represent an ecological adaptation to increasing average surface temperature in central Myanmar (Fig. 13), potentially a widespread phenomenon given that global surface temperatures have increased over the last century with high certainty (IPCC, 2013). Increases in ACL have been applied to infer higher temperature and/or aridity in the source region (Schefuß et al., 2002), as well as supporting evidence to imply rapid warming at the onset of the Paleocene-Eocene thermal maxima (PETM) (Handley et al., 2008; Bush and McInerney, 2015). Potentially, ACL increase within this enclosed hydrological lake basin demonstrates a background signal of increasing temperature within the crater lake catchment or increased airborne *n*-alkane supply from the surrounding arid area.

The potential for preferential short chain *n*-alkane degradation could produce ambiguity in creating a pseudo appearance of vegetation source ACL increase, coincident with increasing surface temperature. However, the consistently high CPI values (above 2) suggest minimal diagenetic

alteration has taken place over the relatively short diagenetic history of the Twin Ma record (Ortiz et al., 2013). Consequently, the signal of increasing ACL is proposed to relate to a combination of biosynthetic adaptation to warmer periods in addition to some potential vegetational composition change and aeolian transport from the surrounding arid catchment. This pattern of increasing ACL towards the present day likely reflects a nonlinear climate signal of increasing mean annual air temperature with high interannual variability in central Myanmar over the 20th century (Fig. 13). It is probable that ACL values falling below the trend line are less representative of the terrestrial catchment but impacted by widespread autochthonous OM production (Fig. 12).

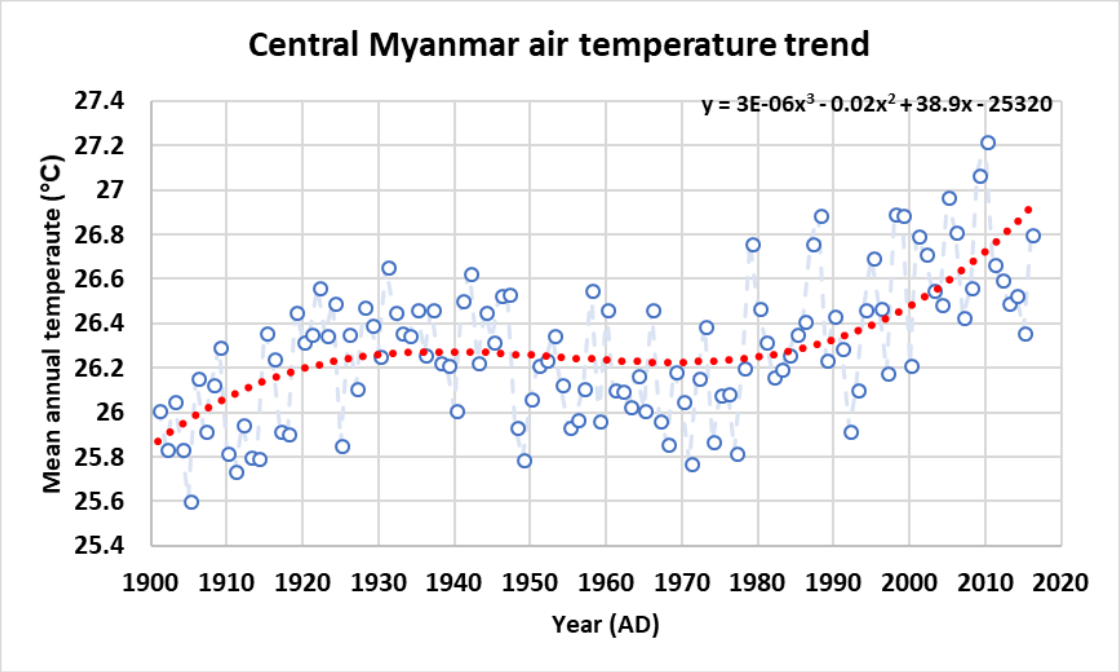

Figure 13. Mean annual air temperature trend in central Myanmar 115-year long CRU TS 4.01 observational climate dataset compiled by Harris et al., (2014) and fitted with a polynomial trendline.

5.4.1. Paleoclimate implication of variation in Twin Ma and Taung Pyauk geochemical proxies

Discerning the climatic signals inferred by changes in OM molecular characteristics provides a complex task in central Myanmar due to its influence by spatially complex overlapping monsoon systems (D'Arrigo and Ummmenhofer., 2014). Both Twin Ma and Taung Pyauk displayed overall trends of various strength indicating oscillatory periods between terrestrial and aquatic vegetational composition. Increased autochthonous OM input was indicated by a characteristic transition to lower ACL and CPI values (Freeman and Pancost, 2014). In Twin Ma, the high resolution recent paleoclimate record allowed the identification of two distinct periods of more aquatic OM input (~ 1925 and 1965) and comparison with other paleoclimate records over the last century.

Geochronological varve studies in the local Twintaung maar lake by Sun et al., (2016) revealed distinct lithogenic (wet season sediment input) and authigenic (dry season carbonate precipitation) layering, producing high and low frequency climate variability in geochemical composition. Distinct periods of increased Paq (decreased ACL) occurred throughout the depth of Taung Pyauk, and around 1925, 1965 and 1990 in Twin Ma; coinciding chronologically with Ca and Sr enrichment in Twintaung (Sun et al., 2016). Strontium can freely substitute into the crystal lattice of calcite or dolomite crystals giving them the tendency to cooccur. Thus, abundance of both Ca and Sr have been widely used as lacustrine proxies to imply increases in calcium carbonate supersaturation (Ω) induced by evaporation and/or increased photosynthetic activity (Kalugin et al., 2013). Correspondingly, D'Arrigo and Ummenhofer, (2014) found negative PDO phases to incur distinguishably lower teak growth around the periods of 1925 and 1965, corresponding reduced moisture flux into central Myanmar (Fig. 14). Combining these results suggest that drier periods with increased evaporation accompany pronounced periodic OM source change to favor increased autochthonous biomass production in an algal/macrophyte dominated waterbody (Fig. 8 & 11).

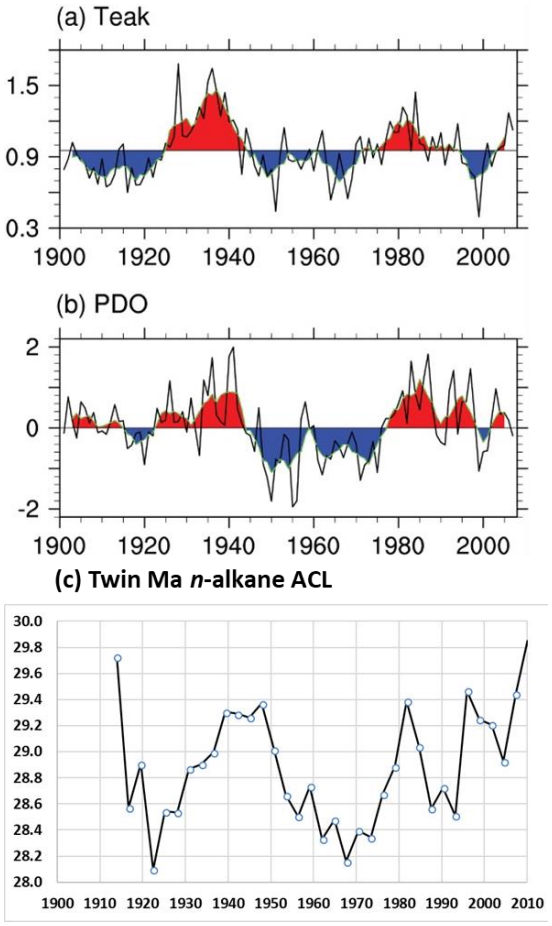

Figure 14. Comparison of Twin Ma n-alkane ACL record with tree-ring width chronology in Central Myanmar and positive (red) and negative (blue) PDO phases. Figure sourced and adapted from D'Arrigo and Ummenhofer, (2014).

In Twin Ma, no *n*-alkane homologues negatively correlated with each other, indicating increasing (decreasing) Paq (ACL) values are caused by autochthonous OM increases in short and mid-chain homologues, without the cutoff of long chain homologue supply. Twin Ma dominant mid-chain n-alkanes C_{19} and C_{23} increases are symbolic of cyanobacteria and submerged or emergent macrophytes respectively (Ortiz et al., 2013). Transition to an algal/macrophyte dominated trophic state likely accompanies a reduction in lake level, triggered by increasing annual evaporation over periodic phases of increased air temperature and reduced precipitation. High autochthonous OM input, indicated by increasing *n*-alkane concentrations, in combination with a steeper pycnocline gradient produces a strongly anoxic hypolimnion upon respiratory oxygen consumption. A rising chemocline and N depletion likely favor N_2 fixing cyanobacteria which further shifts the trophic state to a microbial state during these warm periods (Vázquez et

al 2005; Jia et al., 2011). Consequently, this combination of proxies possibly corresponds to a weaker monsoon, alongside which allochthonous OM supply is reduced and replaced by autochthonous production. The overall dominance of these autochthonous OM dominated periods in Twin Ma supports the findings of Sun et al., (2016) suggesting a weakening monsoon since 1840.

Taung Pyauk provided a longer geochemical record (~ 1500 year) of environmental change supporting higher frequency fluctuation as in Twin Ma, in addition to longer perturbations spanning up to 200 years. This likely corresponds quasi-periodic fluctuations in ENSO, PDO and IOD spanning decadal to sub decadal timescales, alongside longer quasi-centennial (75 to 115-years) and pentadecadal (50 to 70-years) oscillations in PDO (Shen et al., 2016). The typical pattern of reduction (increase) in ACL accompanied by an increase (decrease) in total *n*-alkane concentration, $\delta^{13}C_{TOC}$ and TOC possibly corresponds to less (more) intense monsoonal rainfall over long periods. Shifts to higher $\delta^{13}C_{TOC}$ values is indicative of increased algal and cyanobacterial primary production, as well as increasing abundance of surface dwelling macrophytes (Liu et al., 2013; Mead et al., 2005); implying an extensive period of reduction in waterbody level that is potentially driven by tropical solar forcing and/or tropical sea surface temperature (Sun et al., 2016). Conversely, higher monsoon intensity is likely responsible for the input of more characteristically terrestrial OM into the crater lake catchment under more intense monsoonal periods.

6. Conclusion

Analysis of *n*-alkane compounds extracted from a high resolution 100-year (Twin Ma) and extensive 1500-year maar lake sedimentary record (Taung Pyauk) found high and low frequency fluctuation related to changing monsoon intensity. High average ACL and CPI in both lakes signified an overall terrestrially dominated C_3 and C_4 OM input with minimal diagenetic alteration. In Twin Ma, shifts to lower ACL, CPI and higher total *n*-alkane (C_{17}–C_{40}) concentrations indicated drier monsoonal periods causing trophic level shift to a more cyanobacterial/macrophyte

dominated system with high autochthonous OM production, possibly instigated by quasi-periodic negative PDO phases. A signal of increasing ACL with compiled 3-year average air temperature may indicate increasing biosynthetic affinity for longer chain *n*-alkanes in a warming modern climate.

In the longer Tuang Pyauk record, episodes of quasi-periodic fluctuation of a similar inferred mechanism to Twin Ma were evident, alongside more profound quasi-centennial (75 to 115-years) and pentadecadal (50 to 70-years) periods. Long term episodic $\delta^{13}C_{TOC}$ and TOC increase coupled to decreasing ACL and CPI indicates extended periods of evaporation causing strong physical and chemical stratification with dissolved CO_2 limitation reducing $\delta^{13}C_{TOC}$ fractionation. This inferred environmental reconstruction may indicate that outside of the known quasi-periodic alterations in monsoon intensity, long term episodic fluctuations related to global teleconnections can cause profound environmental change.

Acknowledgements

This thesis would not have been possible without the efforts of many others therefore I would like to express kind appreciation to all. Firstly, I would like to extend my utmost gratitude to my supervisor Rienk Smittenberg for the time, wisdom and guidance that was generously donated readily throughout this thesis project. The sediment core that was kindly provided for this project made this study permittable within the available time, therefore I would like to thank Rienk Smittenberg (IVG), Akkaneewut Chabangborn (IGV, now at Chulalongkorn university, Thailand), Barbara Wohlfarth (IGV), Sherilyn Fritz (University of Nebraska), Zaw Win (Monywa University), Lin Thu (then at University of Yangon), and several student helpers from Monywa University for their efforts on the field expedition in 2013. I would like to acknowledge A. Chabangborn for access to the study site map that was presented in this study. For the subsampling of Taung Pyauk I would like to further thank A. Chabangborn and B. Wohlfarth for their efforts. Acknowledgement is extended to Peerapong Sritangsirikul (Chulalangkorn University) for their time and effort in further processing the Taung Pyauk sediment samples. For analysis of bulk carbon and nitrogen content and stable isotopic composition I acknowledge Heike Sigmund at the Stable Isotope Laboratory (SIL) of Stockholm University and the efforts of P. Sritangsirikul. For help and guidance in the lab I would like to kindly thank Klara Hejndal (IVG) for her generosity and pleasant company. Gratitude is extended to Christophe Dupraz (IVG) for his help and teaching during SEM analysis that made mineralogical analysis possible in this project. I would also like to thank Matt O'Regan for his kind help during the core photography and spectrophotometry analysis. We like to acknowledge Tim Eglinton and Negar Haghipour for 14C analysis at ETH Zurich, and Lars Beckel for 14C analysis at Uppsala University.

References

Ahead, J., Ganeshram, R., Bryant, C., Cisneros-Dozal, L., Ascough, P., Fallick, A. and Slater, G. (2011). Sources of n-alkanes in an urbanized estuary: Insights from molecular distributions and compound-specific stable and radiocarbon isotopes. *Marine Chemistry*, 126(1-4), pp.239-249.

Allen, J., Brandt, U., Brauer, A., Hubberten, H., Huntley, B., Keller, J., Kraml, M., Mackensen, A., Mingram, J., Negendank, J., Nowaczyk, N., Oberhänsli, H., Watts, W., Wulf, S. and Zolitschka, B. (1999). Rapid environmental changes in southern Europe during the last glacial period. *Nature*, 400(6746), pp.740-743.

Bronk Ramsey, C. (2009a). Bayesian analysis of radiocarbon dates. *Radiocarbon*, 51(1), 337-360.

Bronk Ramsey, C. (2008). Deposition models for chronological records. *Quaternary Science Reviews*, 27(1-2), 42-60.

Deaton, W. B. and Damuth, J. (1999). Evaluating optical lightness as a proxy for carbonate content in marine sediment cores. Marine Geology, 161(2-4), pp.141-153.

Bianchi, T. and Canuel, E. (2011). *Chemical biomarkers in aquatic ecosystems*. Princeton: Princeton University Press, p.186.

Brincat, D., Yamada, K., Ishiwatari, R., Uemura, H. and Naraoka, H. (2000). Molecular-isotopic stratigraphy of long-chain n-alkanes in Lake Baikal Holocene and glacial age sediments. *Organic Geochemistry*, 31(4), pp.287-294.

Brocks, J., Love, G., Summons, R., Knoll, A., Logan, G. and Bowden, S. (2005). Biomarker evidence for green and purple sulphur bacteria in a stratified Palaeoproterozoic sea. *Nature*, 437(7060), pp.866-870.

Bush, R. and McInerney, F. (2015). Influence of temperature and C 4 abundance on n -alkane chain length distributions across the central USA. *Organic Geochemistry*, 79, pp.65-73.

Chikaraishi..Y. (2014). $^{13}C/^{12}C$ Signatures in Plants and Algae, in *Treatise in Geochemistry.* pp. 95-123.

Cloud, P.E. Jr. (1962) Environment of calcium carbonate deposition west of Andros Island, Bahamas. *U.S.Geol. Surv Professional Paper* 350, pp 138

Cranwell, P., Eglinton, G. and Robinson, N. (1987). Lipids of aquatic organisms as potential contributors to lacustrine sediments—II. *Organic Geochemistry*, 11(6), pp.513-527.

D'Arrigo, R., Palmer, J., Ummenhofer, C., Kyaw, N. and Krusic, P. (2011). Three centuries of Myanmar monsoon climate variability inferred from teak tree rings. *Geophysical Research Letters*, 38(24).

D'Arrigo, R. and Ummenhofer, C. (2014). The climate of Myanmar: evidence for effects of the Pacific Decadal Oscillation*. International Journal of Climatology*, 35(4), pp.634-640.

Domínguez, E., Cuartero, J. and Heredia, A. (2011). An overview on plant cuticle biomechanics. *Plant Science*, 181(2), pp.77-84.

Eglinton, G. and Hamilton, R. (1967). Leaf Epicuticular Waxes. *Science*, 156(3780), pp.1322-1335.

Fang, J., Wu, F., Xiong, Y., Li, F., Du, X., An, D. and Wang, L. (2014). Source characterization of sedimentary organic matter using molecular and stable carbon isotopic composition of n-alkanes and fatty acids in sediment core from Lake Dianchi, China. *Science of The Total Environment*, 473-474, pp.410-421.

Ficken, K., Li, B., Swain, D. and Eglinton, G. (2000). An n-alkane proxy for the sedimentary input of submerged/floating freshwater aquatic macrophytes. *Organic Geochemistry*, 31(7-8), pp.745-749.

Freeman, K.H. and Pancost R.D. (2014). Biomarkers for Terrestrial Plants and Climate, in *Treatise on Geochemistry*. pp. 395-416.

Hammer, Ø., Harper, D.A.T., and P. D. Ryan, 2001. PAST: Paleontological Statistics Software Package for Education and Data Analysis. Palaeontologia Electronica 4(1): 9pp

Handley, L., Pearson, P., McMillan, I. and Pancost, R. (2008). Large terrestrial and marine carbon and hydrogen isotope excursions in a new Paleocene/Eocene boundary section from Tanzania. Earth and Planetary Science Letters, 275(1-2), pp.17-25.

Harris, I., Jones, P.D., Osborn, T.J. and Lister, D.H. (2014), Updated high-resolution grids of monthly climatic observations – the CRU TS3.10 Dataset. *Int. J. Climatol.*, 34: 623–642. (doi: 10.1002/joc.3711).

Hartmann, D.L., A.M.G. Klein Tank, M. Rusticucci, L.V. Alexander, S. Brönnimann, Y. Charabi, F.J. Dentener, E.J. Dlugokencky, D.R. Easterling, A. Kaplan, B.J. Soden, P.W. Thorne, M. Wild and P.M. Zhai, 2013: Observations: Atmosphere and Surface. In: Climate Change 2013: The Physical Science Basis. Contribution of Working Group I to the Fifth Assessment Report of the Intergovernmental Panel on Climate Change [Stocker, T.F., D. Qin, G.-K. Plattner, M. Tignor, S.K. Allen, J. Boschung, A. Nauels, Y. Xia, V. Bex and P.M. Midgley (eds.)]. Cambridge University Press, Cambridge, United Kingdom and New York, NY, USA.

Hebting, Y. (2006). Biomarker Evidence for a Major Preservation Pathway of Sedimentary Organic Carbon. *Science*, 312(5780), pp.1627-1631.

Htway, O. and Matsumoto, J. (2011). Climatological onset dates of summer monsoon over Myanmar. *International Journal of Climatology*, 31(3), pp.382-393.

Hua, Q., Barbetti, M., & Rakowski, A. J. (2013). Atmospheric Radiocarbon for the Period 1950-2010. *Radiocarbon*, 55(4).

Jia, G., Bai, Y., Yang, X., Xie, L., Wei, G., Ouyang, T., Chu, G., Liu, Z. and Peng, P. (2015). Biogeochemical evidence of Holocene East Asian summer and winter monsoon variability from a tropical maar lake in southern China. *Quaternary Science Reviews*, 111, pp.51-61.

Kalugin, I., Darin, A., Rogozin, D. and Tretyakov, G. (2013). Seasonal and centennial cycles of carbonate mineralisation during the past 2500 years from varved sediment in Lake Shira, South Siberia. *Quaternary International*, 290-291, pp.245-252.

Kennicutt, M., Barker, C., Brooks, J., DeFreitas, D. and Zhu, G. (1987). Selected organic matter source indicators in the Orinoco, Nile and Changjiang deltas. *Organic Geochemistry*, 11(1), pp.41-51.

Liu, W., Li, X., An, Z., Xu, L. and Zhang, Q. (2013). Total organic carbon isotopes: A novel proxy of lake level from Lake Qinghai in the Qinghai–Tibet Plateau, China. Chemical Geology, 347, pp.153-160.

Marzi, R., Torkelson, B. and Olson, R. (1993). A revised carbon preference index. Organic Geochemistry, 20(8), pp.1303-1306.

Mead, R., Xu, Y., Chong, J. and Jaffé, R. (2005). Sediment and soil organic matter source assessment as revealed by the molecular distribution and carbon isotopic composition of n-alkanes. *Organic Geochemistry*, 36(3), pp.363-370.

Miralles, G., Grossi, V., Acquaviva, M., Duran, R., Claude Bertrand, J. and Cuny, P. (2007). Alkane biodegradation and dynamics of phylogenetic subgroups of sulfate-reducing bacteria in an anoxic coastal marine sediment artificially contaminated with oil. *Chemosphere*, 68(7), pp.1327-1334.

Morse, J. W, Millero, F.J., Cornwell, J.C., Rickard, D. (1987). The chemistry of the hydrogen sulfide and iron sulfide systems in natural waters. Deep Sea Research Part B*. Oceanographic Literature Review*, 34(9), p.753.

Nederbragt, A., Dunbar, R., Osborn, A., Palmer, A., Thurow, J. and Wagner, T. (2006). Sediment colour analysis from digital images and correlation with sediment composition. Geological Society, London, Special Publications, 267(1), pp.113-128.]

Neumann, T., Stögbauer, A., Walpersdorf, E., Stüben, D. and Kunzendorf, H. (2002). Stable isotopes in recent sediments of Lake Arendsee, NE Germany: response to eutrophication and remediation measures. *Palaeogeography, Palaeoclimatology, Palaeoecology*, 178(1-2), pp.75-90.

O'Leary, M, H. (1988). Carbon isotopes in photosynthesis. Bioscience 38: 328–336

Ortiz, J., Moreno, L., Torres, T., Vegas, J., Ruiz-Zapata, B., García-Cortés, Á., Galán, L. and Pérez-González, A. (2013). A 220 ka palaeoenvironmental reconstruction of the Fuentillejo maar lake record (Central Spain) using biomarker analysis. Organic Geochemistry, 55, pp.85-97.

Paul Antony, C., Kumaresan, D., Hunger, S., Drake, H., Murrell, J. and Shouche, Y. (2012). Microbiology of Lonar Lake and other soda lakes. *The ISME Journal*, 7(3), pp.468-476.

Pike, J. and Kemp, A. (1996). Preparation and analysis techniques for studies of laminated sediments. *Geological Society*, London, Special Publications, 116(1), pp.37-48.

Rau, G. H., Riebesell. U and Wolfgladrow. D. (1997). CO2aq-dependent photosynthetic δ13C fractionation in the ocean: A model versus measurements. *Global Biogeochemical Cycles* 11: pp. 267–278.

Reimer, P. J., Bard, E., Bayliss, A., Beck, J. W., Blackwell, P. G., Bronk Ramsey, C., Grootes, P. M., Guilderson, T. P., Haflidason, H., Hajdas, I., HattŽ, C., Heaton, T. J., Hoffmann, D. L., Hogg, A. G., Hughen, K. A., Kaiser, K. F., Kromer, B., Manning, S. W., Niu, M., Reimer, R. W., Richards, D. A., Scott, E. M., Southon, J. R., Staff, R. A., Turney, C. S. M., & van der Plicht, J. (2013). IntCal13 and Marine13 Radiocarbon Age Calibration Curves 0-50,000 Years cal BP. *Radiocarbon*, 55(4).

Robinson, D. (2001). δ15N as an integrator of the nitrogen cycle. *Trends in Ecology & Evolution*, 16(3), pp.153-162.

Schefuß, E., Ratmeyer, V., Stuut, J., Jansen, J. and Sinninghe Damsté, J. (2003). Carbon isotope analyses of n-alkanes in dust from the lower atmosphere over the central eastern Atlantic. *Geochimica et Cosmochimica Acta*, 67(10), pp.1757-1767.

Sen Roy, N. and Kaur, S. (2000). Climatology of monsoon rains of Myanmar (Burma). International Journal of Climatology, 20(8), pp.913-928.

Sen Roy, S. and Sen Roy, N. (2010). Influence of Pacific decadal oscillation and El Niño Southern oscillation on the summer monsoon precipitation in Myanmar. *International Journal of Climatology*, 31(1), pp.14-21.

Shen, C., Wang, W., Gong, W. and Hao, Z. (2006). A Pacific Decadal Oscillation record since 1470 AD reconstructed from proxy data of summer rainfall over eastern China. *Geophysical Research Letters*, 33(3).

Simoneit, B., Cardoso, J. and Robinson, N. (1991). An assessment of terrestrial higher molecular weight lipid compounds in aerosol particulate matter over the south atlantic from about 30–70°S.

Sinninghe Damsté, J., Wakeham, S., Kohnen, M., Hayes, J. and de Leeuw, J. (1993). A 6,000–year sedimentary molecular record of chemocline excursions in the Black Sea. Nature, 362(6423), pp.827-829.

Sun, Q., Shan, Y., Sein, K., Su, Y., Zhu, Q., Wang, L., Sun, J., Gu, Z. and Chu, G. (2016). A 530 year long record of the Indian Summer Monsoon from carbonate varves in Maar Lake Twintaung, Myanmar. *Journal of Geophysical Research: Atmospheres*, 121(10), pp.5620-5630.

Sun, Q., Xie, M., Shi, L., Zhang, Z., Lin, Y., Shang, W., Wang, K., Li, W., Liu, J. and Chu, G. (2013). Alkanes, compound-specific carbon isotope measures and climate variation during the last millennium from varved sediments of Lake Xiaolongwan, northeast China. Journal of Paleolimnology, 50(3), pp.331-344.

Tuo, J., Wu, C., Zhang, M. and Chen, R. (2011). Distribution and carbon isotope composition of lipid biomarkers in Lake Erhai and Lake Gahai sediments on the Tibetan Plateau. *Journal of Great Lakes Research*, 37(3), pp.447-455.

Vázquez, G., Jiménez, S., Favila, M. and Martínez, A. (2005). Seasonal dynamics of the phytoplankton community and cyanobacterial dominance in a eutrophic crater lake in Los Tuxtlas, Mexico*. Écoscience*, 12(4), pp.485-493.

Vogts, A., Schefuß, E., Badewien, T. and Rullkötter, J. (2012). n-Alkane parameters from a deep sea sediment transect off southwest Africa reflect continental vegetation and climate conditions. *Organic Geochemistry*, 47, pp.109-119.

Widdel, F. and Rabus, R. (2001). Anaerobic biodegradation of saturated and aromatic hydrocarbons. *Current Opinion in Biotechnology*, 12(3), pp.259-276.

Zech, M., Krause, T., Meszner, S. and Faust, D. (2013). Incorrect when uncorrected: Reconstructing vegetation history using n-alkane biomarkers in loess-paleosol sequences – A case study from the Saxonian loess region, Germany. *Quaternary International*, 296, pp.108-116.

Zhang, Y., Su, Y., Liu, Z., Yu, J. and Jin, M. (2017). Lipid biomarker evidence for determining the origin and distribution of organic matter in surface sediments of Lake Taihu, Eastern China. *Ecological Indicators*, 77, pp.397-408.

Appendix

Appendix 1. Sample site and sediment core photographs

Taung Pyauk

Twin Ma

Appendix 1. Taung Pyauk and Twin Ma lake sample sites and core photographs

Appendix 2. Core splitting and subsampling photographs

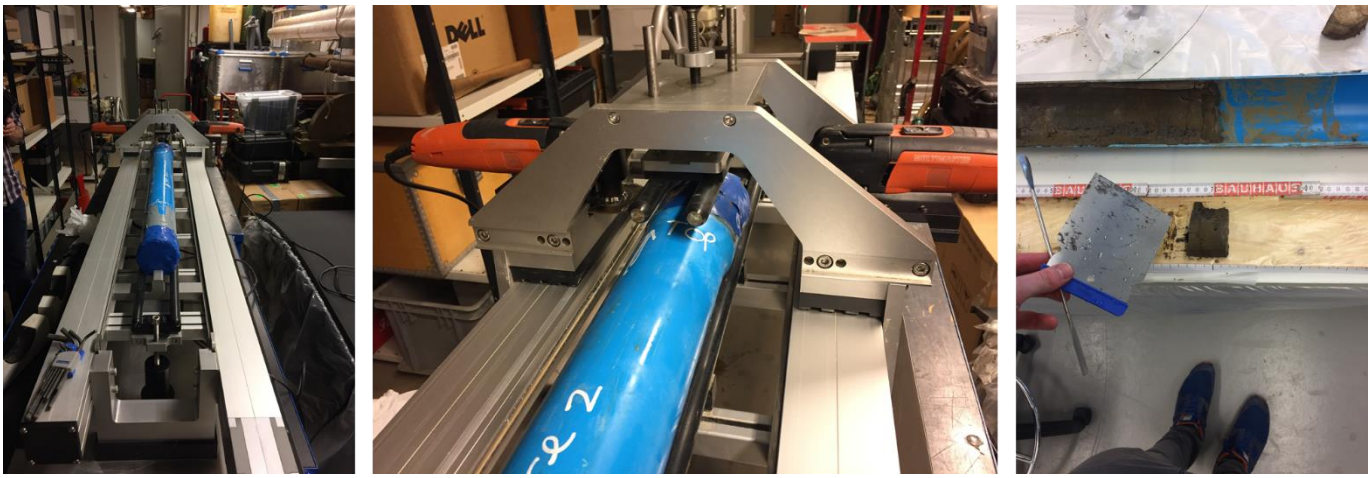

Appendix 2. Core splitting and sediment subsampling stages

Appendix 3. Identified compounds of interest and associated mass spectra

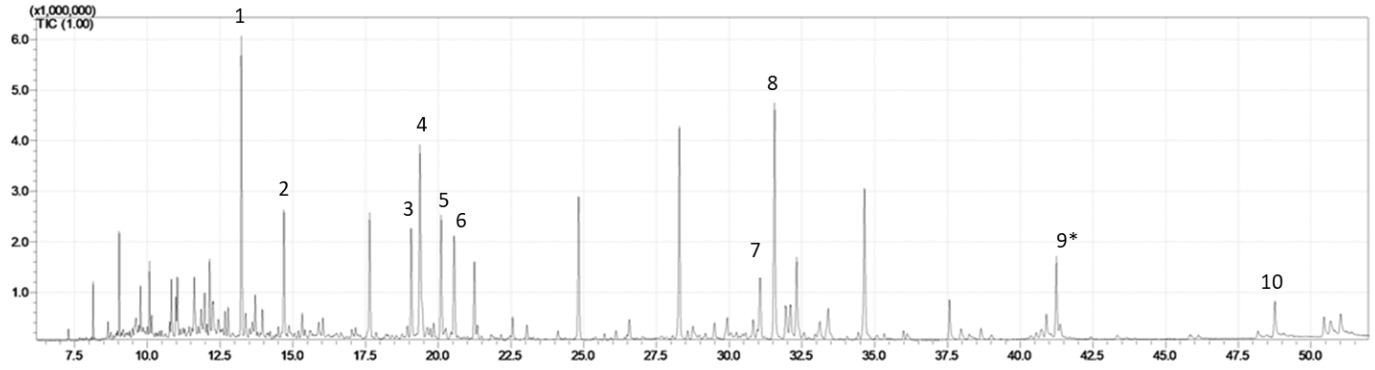

Appendix 3. 10 compounds of interest that were identified and quantified. Only compound 9 (123 m/z characteristic peak and 552 total mass) was further analysed and described. All mass spectra are displayed below.

1

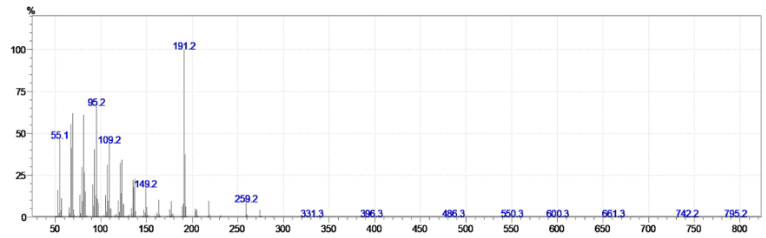

2

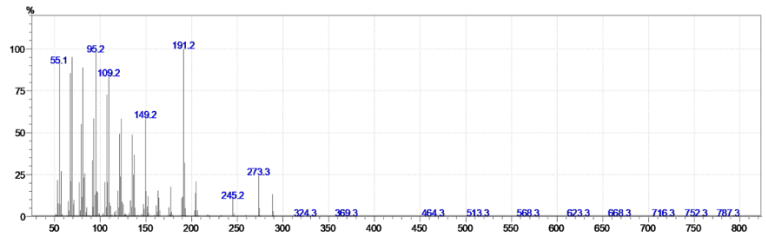

3

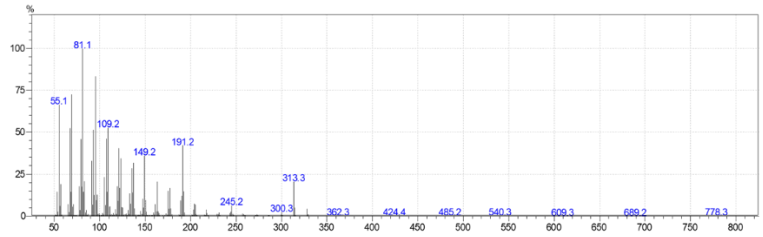

4

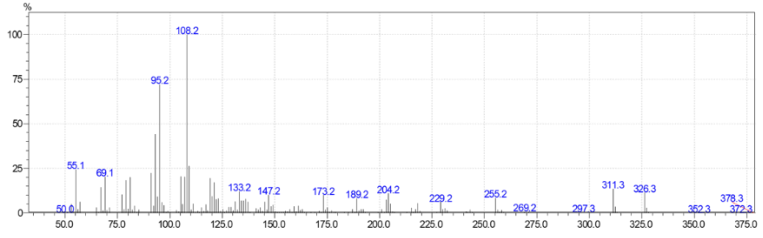

5

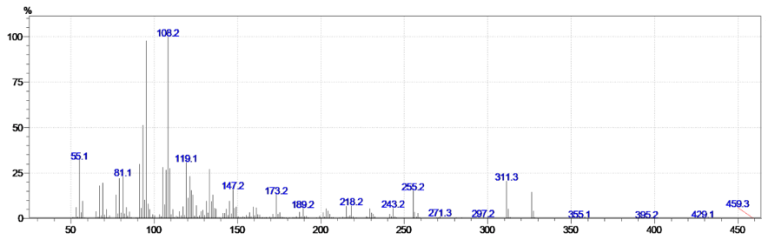

6

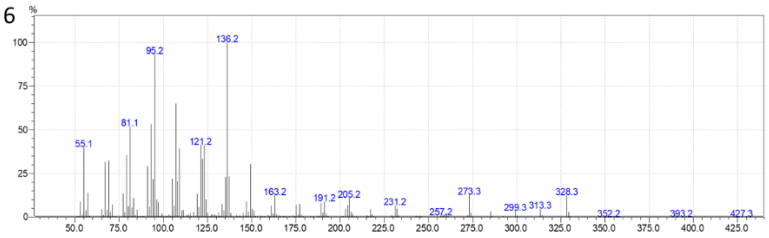

7

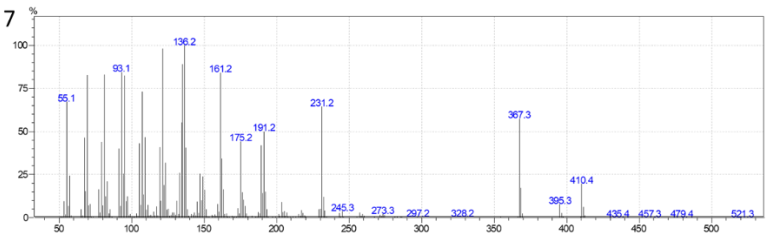

8

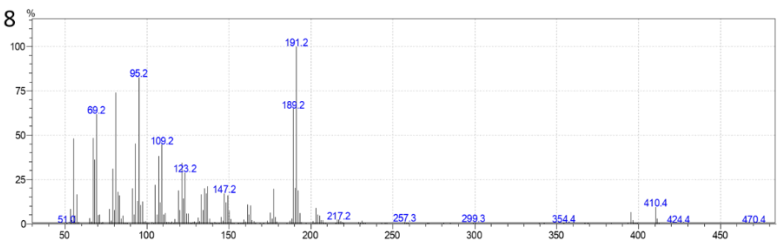

9*

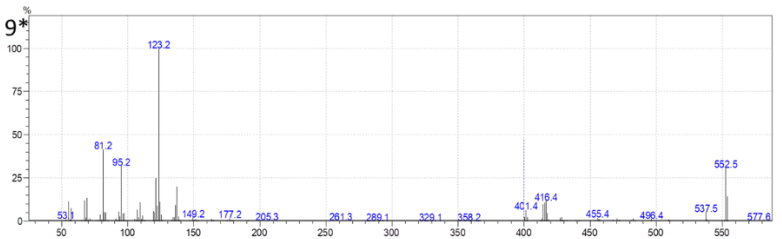

10

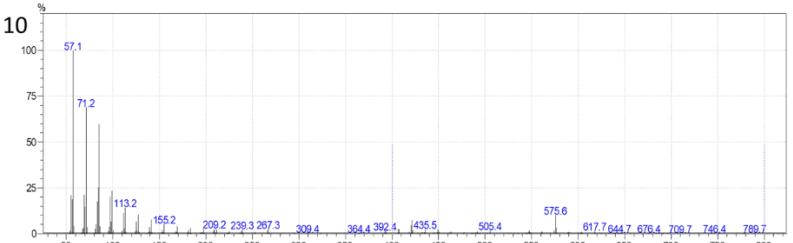

Appendix 4. GCMS Postrun Analysis Peak Quantification Method

The following method describes the automated peak integration method used for n-Alkane sample analysis using the GCMS Postrun Analysis program of the Shimadzu GCMS-QP2010 ultra machine. The section describes the creation of a method with a fixed compound table from an n-alkane standard that can be used to identify and quantify n-alkane peaks. For identification of compounds not present in the external standard, the same method was used but using an example sample containing desired compound peaks to formulate a compound table to be used on the sample batch.

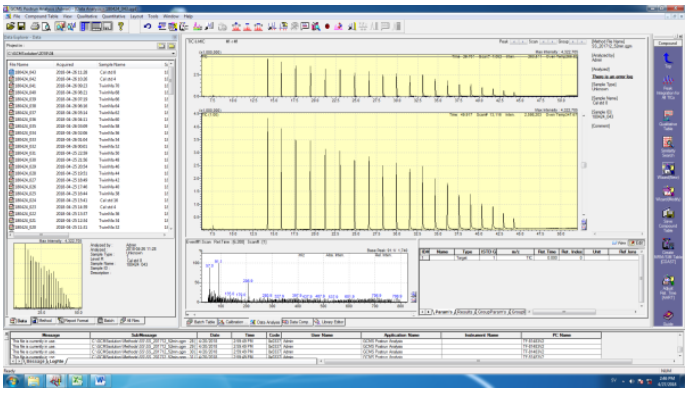

1. A n-alkane external standard was loaded in the 'Data Analysis' tab to form a template from which n-alkane peaks can be automatically quantified. A compound table was created via the compound table wizard (New) tab, allowing a new method to be created.

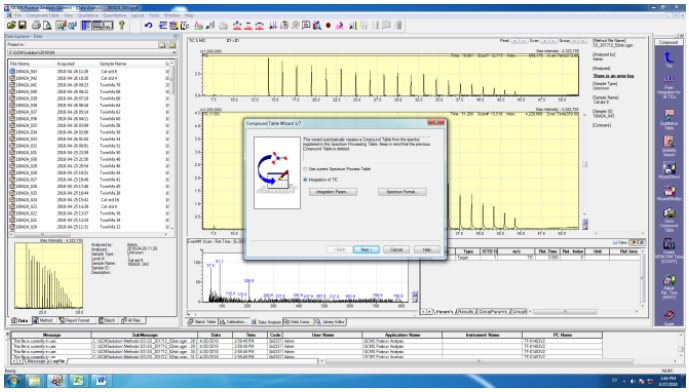

2. In the Compound Table Wizard an integration of TIC (Total Ion Chromatograph) is selected. Integration parameters can be set in the 'Integration Parameters' tab and an integration can be simulated in the 'Spectrum Format' tab.

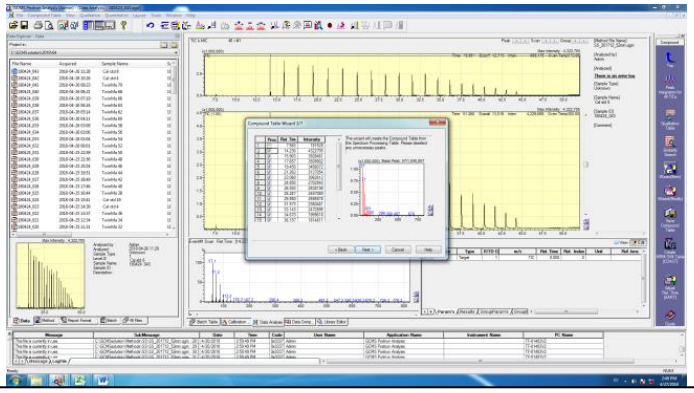

3. By pressing next, a peak integration is simulated from the n-Alkane standard. Clicking on each box displays the associated peak with a vertical line in the window chromatograph window behind, along with an adjacent mass spectrum. Required peaks can be selected or deselected depending on the desired compounds, for n-alkane analysis peaks C_{21} to C_{40} were selected.

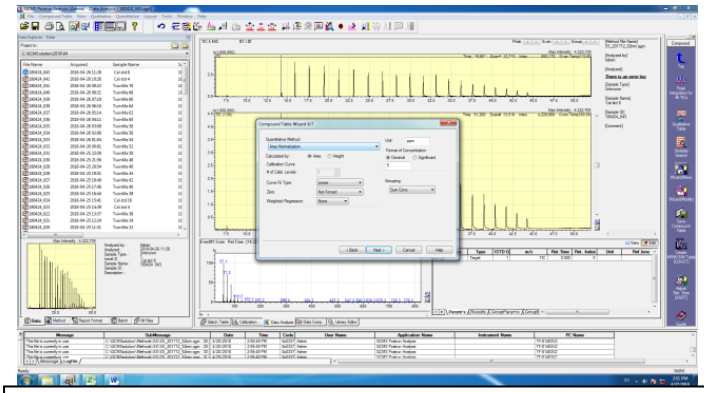

4. The 'Area Normalisation' quantification was selected to give an associated peak area to each compound peak so that a later calibration could be performed to calculate a concentration of each compound within samples.

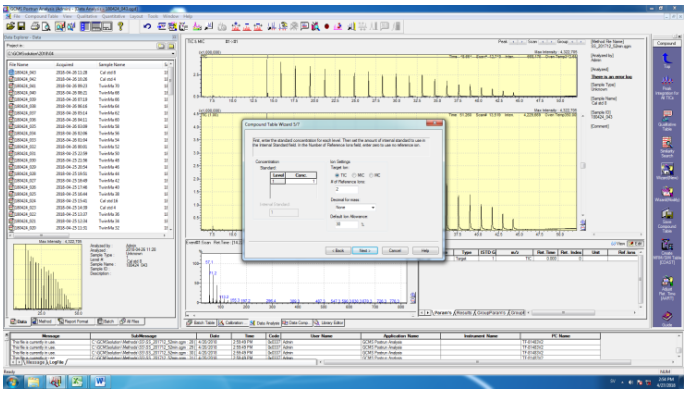

5. The TIC target ion setting was selected with 2 target ions used for compound identification. The automatic calibration step was skipped, and an external calibration used instead. Before completing the compound table wizard, each compound was named according to its hydrocarbon chain length.

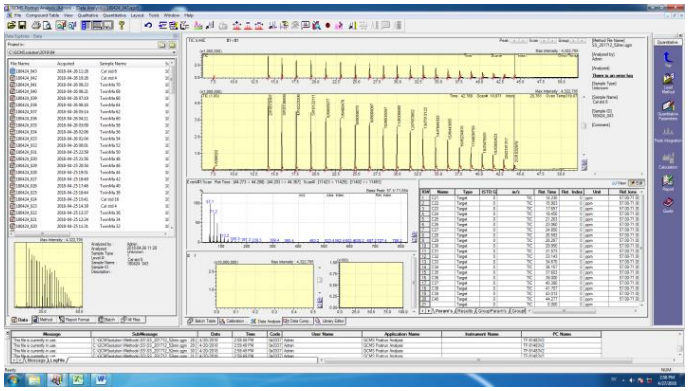

6. Once completed, the compound table can be saved and a 'Peak Integration for all ID's' can be completed to simulate the automatic integration, from which the results are displayed in the results tab.

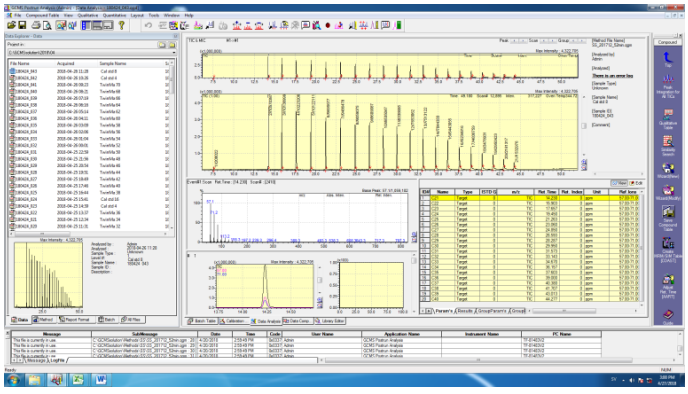

7. The completed results can be viewed along with associated chromatogram peaks.

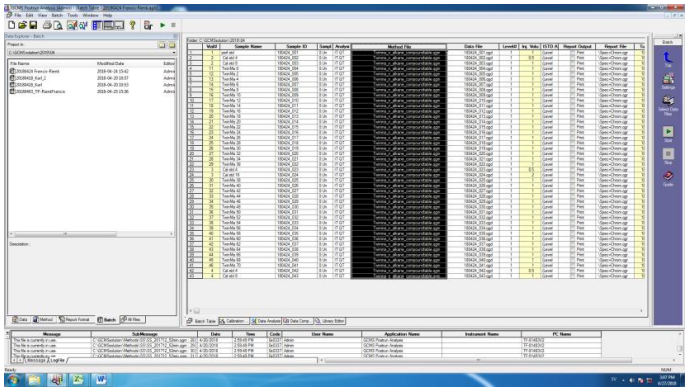

8. Once a satisfactory method for peak integration was created a batch process was undertaken by loading the saved method in the 'Method File' column.

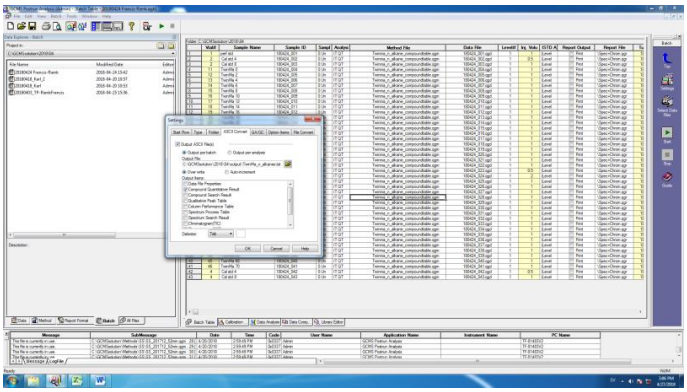

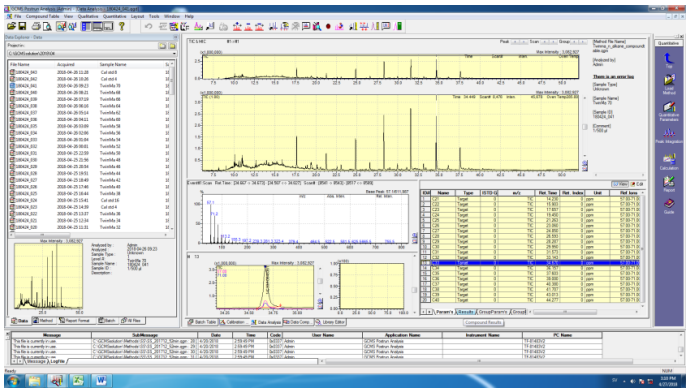

9. Before running a batch quantification, in the Batch/Settings/ASCII convert tab, an ASCII conversion of the Compound Quantitative Result into a selected output file was undertaken. This allowed efficient data export into Excel for later analysis. Once this stage was completed the batch can be processed via 'Start'.

10. Upon batch processing, the integration results can be viewed in the 'Data Analysis' tab. The batch results were exported into Excel for further analysis.

Appendix 5. Normality tests of relevant parameters

Taung Pyauk distribution	Paq	ACL	CPI	total n-alkanes ug g^{-1} se
N	79	79	79	79
Shapiro-Wilk W	0.99	0.99	0.84	0.99
p(normal)	0.69	0.86	**0.00000009**	0.51
	C23	δ13Corg vs PDB (‰)	% Corg	δ15N vs AIR (‰)
N	79	80	80	80
Shapiro-Wilk W	0.95	0.9161	0.9562	0.98
p(normal)	**0.002**	**0.00006**	**0.008**	0.24

Twin Ma distribution	Paq	ACL	CPI	total n-alkanes ug g^{-1} sed	C23	Biomarker X
N	36	36	36	36	36	24
Shapiro-Wilk W	0.97	0.97	0.93	0.85	0.89	0.7
p(normal)	0.55	0.53	**0.022**	0.20	0.14	0.00004

Appendix 5. All relevant normality tests for statistical analysis undertaken. The failing of the Shapiro-Wilk assumption of normality resulted in the use of non-parametric statistical tests.

Appendix 6. Taung Pyauk typical UCM examples

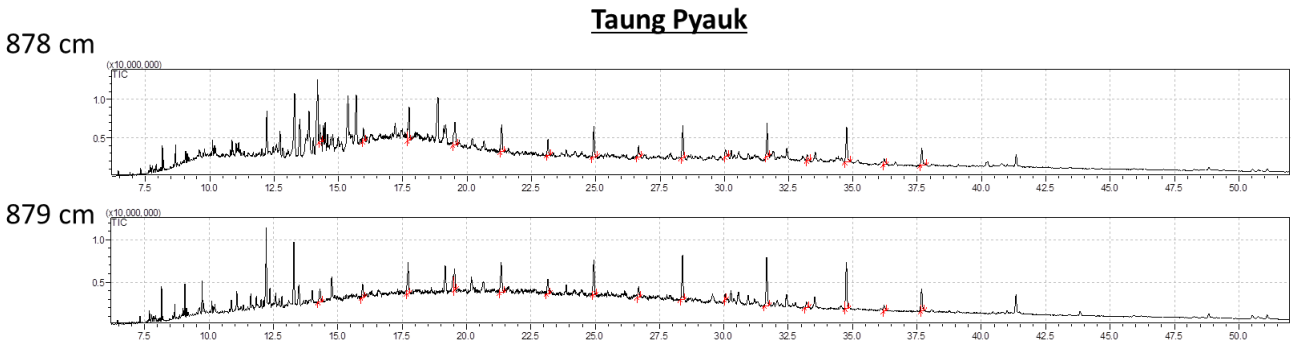

Appendix 6. Typical examples of UCM found in Taung Pyauk. Red targets indicate manually integrated peaks.